Miray ÜNLÜ QUANTUM DOT BASED BIOSENSING AGU 2017

QUANTUM DOT BASED BIOSENSING

A Master's Thesis

By
Miray ÜNLÜ
July 2017

ABDULLAH GÜL UNIVERSITY

QUANTUM DOT
BASED BIOSENSING

A THESIS
SUBMITTED TO THE DEPARTMENT OF ADVANCED MATERIALS AND NANOTECHNOLOGY AND THE GRADUATE SCHOOL OF ENGINEERING AND SCIENCES OF ABDULLAH GÜL UNIVERSITY
IN PARTIAL FULFILLMENT OF THE REQUIREMENTS
FOR THE DEGREE OF
MASTER OF SCIENCE

By
Miray ÜNLÜ
July 2017

SCIENTIFIC ETHICS COMPLIANCE

I hereby declare that all information in this document has been obtained in accordance with academic rules and ethical conduct. I also declare that, as required by these rules and conduct, I have fully cited and referenced all materials and results that are not original to this work.

Miray ÜNLÜ

REGULATORY COMPLIANCE

M.Sc. thesis titled “Quantum Dot Based Biosensing” has been prepared in accordance with the Thesis Writing Guidelines of the Abdullah Gül University, Graduate School of Engineering and Science.

Prepared By	Advisor
Miray ÜNLÜ	Assist. Prof. Evren Mutlugün

Head of the Advanced Materials and Nanotechnology Program
Prof. Murat DURANDURDU

ACCEPTANCE AND APPROVAL

M.Sc. thesis titled “Quantum Dot Based Biosensing” was prepared by Miray ÜNLÜ, which has been accepted by the jury in the Advanced Materials and Nanotechnology Graduate Program at Abdullah Gül University, Graduate School of Engineering and Science.

…../…/2017

JURY:

Advisor : Assist. Prof. Evren MUTLUGÜN

Member : Assoc. Prof. Hakan USTA

Member : Assoc. Prof. M. Serdar ÖNSES

APPROVAL:

The acceptance of this M.Sc. thesis has been approved by the decision of the Abdullah Gül University, Graduate School of Engineering and Science, Executive Board dated ….. /….. / …….. and numbered ……..……. .

Graduate School Dean
Prof. İrfan ALAN

ABSTRACT

QUANTUM DOT BASED BIOSENSING

Miray ÜNLÜ

M.Sc. in Advanced Materials and Nanotechnology

Supervisor: Assist. Prof. Evren MUTLUGÜN

July 2017

Semiconductor nanocrytals also known as quantum dots (QD) with high photoluminesce quantum yield (PLQY), size tunability and favorable optical characteristics occupy a significant area in display technology, solar energy conversion and bioapplications. Size tuning feature of QDs allows emission wavelength ranging from ultraviolet to infrared spectral region. In literature, QD based studies have been performed in visible spectral range by employing mostly cadmium, being a toxic heavy metal. Recently, the search for less toxic alternatives revealed the cadmium free compounds, particularly InP. Cadmium free semiconductor nanocrytals' potential to be used as fluorescent probes in biodetection and biolabeling area has been proved over the past decades.

Pathogens threaten life particularly via water sources like rivers, reservoirs and groundwater. Increasing demand for managing the 'contamination of drinkable water by pathogenic bacteria' problem needs a broad perspective about pathogens and their membrane characteristics which are integral part of microorganism detection platforms.

Bacteria are categorized mainly upon their membrane properties which are gram negative and gram positive. Extra wall called as peptidoglycan layer in gram positive bacteria makes them more resistant to external forces. Gram negative bacteria with wavy wall is relatively more prone to their environment. One of the most known pathogenic bacteria, E. Coli, have damaged and destroyed many lives throughout the world. High growth rate enables this microorganism to spread around large areas in short time. Therefore, accurate and definite detection of this bacteria in water is crucial.

The main frame of this research depends on QD based biodetection of bacteria. First of all, organic based QDs (50% PLQY) containing triocytlyphosphine-sulfur ligand were

synthesized and via successful phase transfer, aqueous QDs with 20% PLQY were achieved. Although surface is damaged during ligand exchange procedure, aqueous QDs with high PLQY were obtained. SiO_2 was covered with QDs thanks to the attraction between their NH_2 group and carboxylic ends, respectively. In the final step, this hybrid structure was covered with SiO_2 and silica coated QDs (SCQD) were formed. In order to utilize SCQDs in bacteria detection, fluorescent agents were embeded in polymeric films which were formed by spin coating. As a result, SCQD facilitates the attachment of negatively charged bacteria onto the surface of the films.

Appropriately grown DH5 alpha (E. Coli strain) expressing green fluorescent protein (GFP) was used as pathogen in the detection part. SCQD thin films were treated with water containing E.Coli DH5 alpha. Positively charged SCQD attracted negatively charged bacteria and the conjugation between them was analysed with time resolved spectroscopy and monitored with fluorescence microscope. Thus, usage of QDs as biosensor in pathogen detection could provide an insight in the future studies.

Keywords: biodetection, E.coli, quantum dots, semiconductors, silica coated quantum dots, indium phosphate, InP QD

ÖZET
KUANTUM NOKTA TEMELLİ BİYOALGILAMA

Miray ÜNLÜ
İleri Malzemeler ve Nanoteknoloji Anabilim Dalı Yüksek Lisans
Tez Yöneticisi: Yrd. Doç. Dr. Evren MUTLUGÜN

Temmuz 2017

Kuantum noktacık olarak adlandırılan yarı iletken nanokristaller yüksek fotolüminesans verimi, değiştirilebilir boyut ve üstün optik özellikleri ile ekran teknolojileri, güneş panelleri ve biyouygulamalarda önemli bir yere sahiptir. Emisyon dalga doyu spektrumu ultraviyole bölgeden kızılötesi bölgeye kadar uzanmaktadır. Literatürde QD tabanlı çalışmalar görünür spektral alanda, özellikle toksik ve ağır bir metal olan kadmiyum kullanılarak gerçekleştirilmektedir. Düşük toksisiteye sahip alternatiflerin arayışı InP gibi kadmiyum içermeyen bileşikleri ortaya çıkarmıştır. Kadmiyum içermeyen kuantum noktacıkların biyoalgılama ve biyoişaretleme alanlarında floresan ajanlar olarak kullanım potansiyeli son yıllarda yapılan çalışmalarla ortaya konmuştur.

Patojenler canlıları su üzerinden özellikle nehir, yeraltı kaynakları ve rezervler yoluyla tehdit etmektedir. Patojenik bakteriler tarafından yapılan kontaminasyon tüm dünyayı endişelendiren bir olgu haline gelmiştir. Bu probleme yönelik çözüm arayışları, bakteriler ve onların tespiti için kritik öneme sahip olan membran özelliklerinin geniş bir perspektifte ele alınmasını gerektirmektedir.

Bakteriler genellikle membran yapılarına göre (gram pozitif ve gram negatif) sınıflandırılmaktadır. Peptidoglikan tabaka olarak da adlandırılan ekstra hücre duvarı gram pozitif bakterileri çevresine karşı daha dirençli yapmaktadır. İnce bir duvarla çevrili olan gram negatif bakteriler ise dışarıdan gelen etkilere daha açıktır. En iyi bilinen patojenik bakteri türlerinden biri olan E. Koli şimdiye kadar dünya çapında

birçok yaşamı tehdit etmiş ve zarar vermiştir. Yüksek çoğalma kapasitesi bu mikroorganizmanın kısa sürede büyük alanlara yayılmasına imkan vermektedir. Bu sebeplerden dolayı su kaynaklarındaki bakterilerin doğru ve kesin tespiti elzemdir.

Bu çalışmanın ana iskeletini bakterilerin kuantum noktacık bazlı biyoalgılaması oluşturmaktadır. Öncelikle triositilfosfin-sülfür ligandına sahip kuantum noktacıklar (50% ışıma verimi) sentezlendi ve başarılı bir faz transferi ile su bazlı (20% ışıma verimi) kuantum noktacıklar hazırlandı. Ligand değişimi sırasında ortaya çıkan yüzey hasarına rağmen, yüksek verimle ışıyan su bazlı kuantum noktacıklar elde edildi. NH_2 kaplı SiO_2, yüzey etkileşimi yaratan karboksilik ligandlara sahip kuantum noktacıklar ile kaplandı. Bu parçacıkların üzerine tekrar SiO_2 kaplanarak silika içeren kuantum noktacık yapıları oluşturuldu. Bu yapıların bakteri tespitinde kullanılması floresan ajanların dönel kaplama yöntemiyle hazırlanan polimerik filmlerin içerisine gömülmesiyle sağlandı.

Uygun bir şekilde büyütülen yeşil floresan protein sentezleyen DH5 alfa (E. Koli ırkı) algılama için patojen olarak kullanıldı. Silika kaplı hibrit yapıyı içeren polimerik filmler içerisinde E. Koli DH5 alfa bulunduran su ile muamele edildi. Pozitif yüklü hibrit yapı ile negatif yüklü bakteri arasındaki etkileşim zaman çözünürlüklü spektroskopi ve floresan mikroskobu ile analiz edildi. Böylece, kuantum noktacıkların patojen biyoalgılamada sensör olarak kullanılabileceği gösterilmiş ve gelecek çalışmalara ışık tutması amaçlanmıştır.

Anahtar kelimeler: biyoalgılama E.koli, kuantum noktacık, yarıiletkenler, silika kaplı kuantum noktacıklar, indiyum fosfat, InP QD

Acknowledgements

At first, I would like to express my deepest appreciation to my advisor, Assist. Prof. Evren Mutlugün. His support and encouragement gave me strength and assurance. Prof. Mutlugün's deep knowledge and enthusiasm for science has had such an intense impact on me and my career. My research would not have been possible without his guidance and efforts.

I would like to acknowledge that this study was supported by TUBITAK Project (114E107) and Bilkent/UNAM and Urartu Şeker as principle investigator of Synthetic Biosystems and Bionanotechnology Laboratory.

Finally, I would like to thank my family with my all heart; my precious parents, my dear brother for their strong motivation.

Table of Contents

List of Figures

List of Tables

Chapter 1

Introduction

1.1 Quantum Dots

Quantum dots (QD), also known as semiconductor nanocrystals are building blocks in nanoscale dimesion (2-20 nanometer). QD indicates promising approachs in solar cells [1], in vivo imaging [2], photodetection [3] due to having narrow and size tunable emission characteristics with broad absorption and excitation spectrum.

Discovery of QD dates back to 1980s [4]. Concentration on NCs proceeded by breakthrough phenomenon called as quantum size effect of semiconductors in optic spectral level [4] [5]. Glass matrices were used to compile optic data of QD. However, adjustable physical and chemical characteristic, uniformity, size tunability took a decade. In 1993, hot injection technique authorized by Bawendi group enabled production of highly monodispersed cadmium based QDs [6].

Non-aqueous surfactant such as organic solvents are comprised in colloidal synthesis. The term nanoparticle demonstrates the size of approximately 1-100 nm. Quantum dots with less than 20 nm sized hallmark are defined as a piece of matter that confine electrons and holes in 3D dimension.

Colloidal synthesis of semiconductor nanocrystals are based on high and low temperature route. While hot injection technique, a kind of high temperature process, maintains temperature approximately at 300 °C for QD growth, low temperature method keeps temperature relatively at 90 °C. High temperature technique results in better PLQY efficiency with highly monodispersed QD particles compared to low temperature route [7] [8].

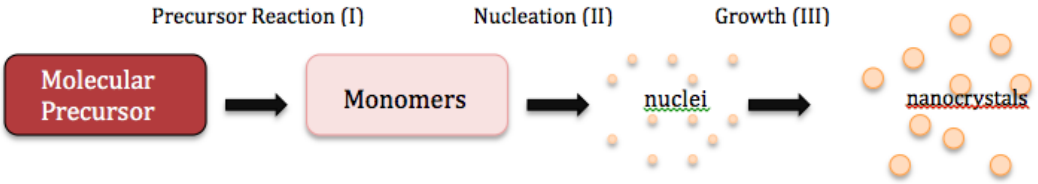

Figure 1.1.1 Basic growth process of nanocrystals [9]

Molecular precursor introducing into the reaction mixture initiates the monomer formation which culminate in nucleation [10]. Growth process continues with the flowing of monomers onto nanocrystal surface (Figure 1.1.1). Ostwald ripening [11] may take place in case of monomer concentration depletion by dissolving of small dots to form larger ones (Figure 1.1.2). These steps could change with the introduction of stabilizers which adhere to the dot surface and give chemical and colloidal stability to NCs.

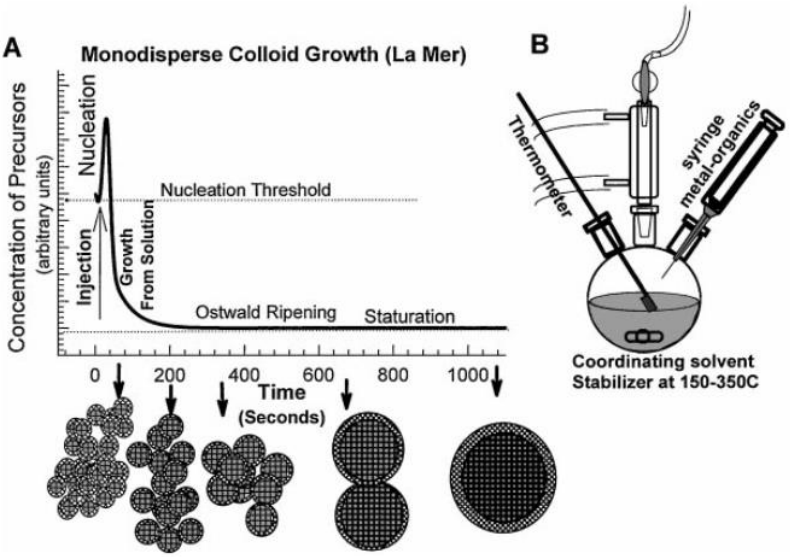

Figure 1.1.2 Colloidal quantum dots. (a) Crystallographic model and (b) CdSe QD (high resolution TEM image). (c) Chemical synthesis setup of colloidal QDs (d) Illustration of NC synthesis regarding concentration of the monomers [5]

Upon reaching the nucleation threshold, fast nucleation occurs with the hot injection method which induce rapid production of monomers. Optimal precursor theory explains the bacis principles of hot injection tecnique [5].

As nucleation rate is defined at *dN/dt:*

$$\boldsymbol{dN/dT = Aexp(-\Delta G^N/RT)} \qquad (1.1.1\text{-}1)$$

ΔG^N is the activation energy related to $16\pi\gamma^3 V_m{}^2/3(RT \ln S)^2$, γ is the surface energy, V_m is the molar volume, S is the supersaturation. S = [Monomer] C^O . Highly reactive precursors are required in a short period of time at a specific temperature. Metal compounds such as PbSnTe [12], Fe_2O_3 [13], cheaper, less air sensitive Cd chalcogenide [14] ; non-metal precursors such as trimethylsilyl, alkylphophine related chemicals are also used for efficient NC production. Capping ligands (myristic acid [15], trioctylphosphine [16]) are stabilizers of the reaction, also can perform as coordinating solvent such as hexadecylamine [17].

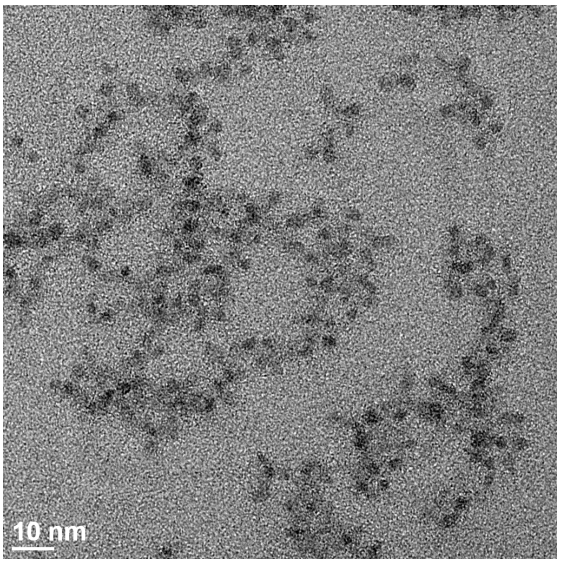

Figure 1.1.3 a) Optical micrograph of colloidal InP/ZnS nanocrystals

1.1.1 Surface chemistry

Photophysical characteristic of inorganic NCs makes explicit response to surface passivation and defective problems so proper ligand selection is one of the fundamental issue in light driven processes in QDs. Donor and acceptor dependent RET efficiency was studied by removing surface ligands with an insulating shell. Drastic quenching of RET were observed in that research [18].

Besides the crucial effect on nucleation and growth, adherence of surface ligands to the

surface supports the interparticle attraction such as electrostatic interaction and dissolving in certain solvents. Mostly used ligands in the formation of NCs are the organic hydrocarbon molecules. Even as providing high chemical flexibility to crystals, these long chain molecules mostly block the charge transport [19]. On the other hand, total removal of ligands cause destruction of surface dangling bonds which provides carrier trapping in NCs [20]. With slightly removal of ligands and ligand exchange methods, accessing the target NCs is possible nowadays.

1.1.2 Organic capping ligands

Surfactants as initial capping includes anchoring chemical groups such as amino, sulfonato, thio and alkyl or aromatic based ones [21]. Instead, steric stabilization of II-IV semiconductor NCs (CdTe, HgTe) is constructed with a thiol and a charged group. High luminescence emission of QDs with charge stabilizer has so far limited to thiolgycol based ones [22]. Binding mechanism of NC and ligand status has not been completed yet due to missing part of analytical tools to discover the surface atomic structure of these crystals. In metal ligand materials and salts binding type is known. For example, olate like anionic material bind cationic surfaces [23] (Cd^{2+}).

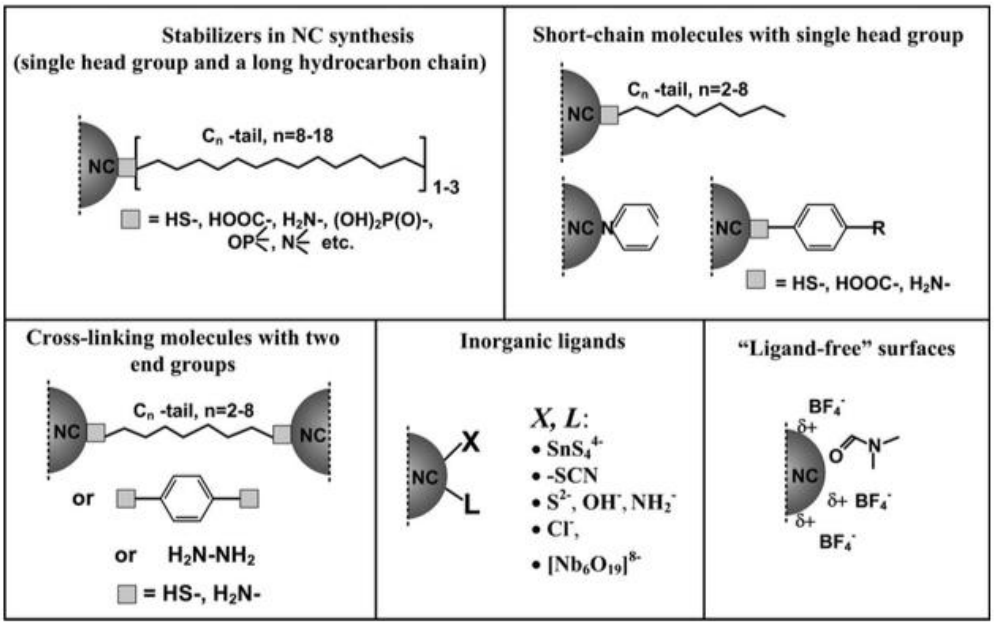

Figure 1.1.2.1 Frequently used organic & inorganic ligand attachment to the NC surface [24]

1.1.3 Ligand exchange molecules

Initial long chain ligand exchange procedure depends on two stages: removal of initial capping molecules and introducing new short chain ligand into the solution. Ligand exchange-phase transfer process is limited with the diminish of colloidal stability and emission capacity. Nanoparticle aggregation is also another drawback of these kind of transfer strategy. To enhance the quality of NC which is embedded into film in several applications, amine- based or pyridine type solutions are used by soaking of CdSe or PbSe QD films into the solution [25], [26]. The improvement of photoconductivity (10^{12}-10^{13} Jones) by PbS QD film in butylamine solution is maintained due to decreasing inter NC spacing [27]. In addition, capping ligands polythiophene [28] like electrically conjugated polymers enhance the electrical characteristics of NCs.

1.1.4 Inorganic capping ligands

Metal chalcogenide complexes (MCCs) such as SnS_4, In_2Se_4 can behave like surface capping ligands. The terminal chalcogenide atoms have high chemical affinity to electron deficient surface of NCs. Transfer of MCCs by removing organic ligands from the NC surface, provide high chemical stability and solubility in formamide and hydrazine like polar solvents with high dielectric constant. In a study, halide (Cl^-, Br^-, I^-) ligands were used to passivate the NCs with alkylphosponate following treating NC films with alkylamonium halides. Stable colloidal QDs were obtained [29].

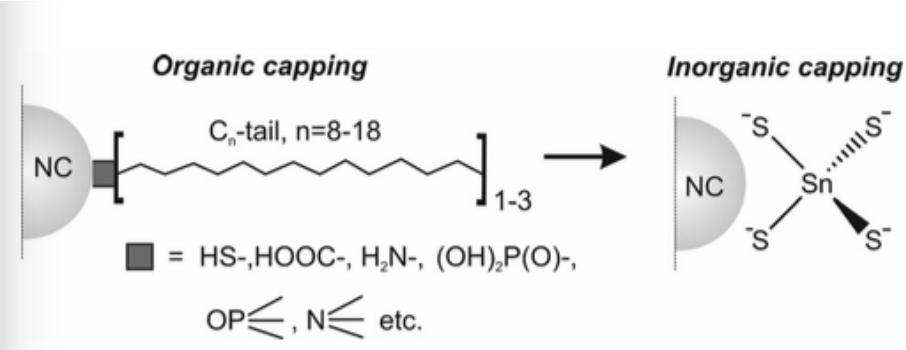

Figure 1.1.4.1 Ligand exchange process by transferring capping molecules from organic to inorganic terminal end [30]

1.1.5 Bare NC surfaces

Ligand free NCs have many drawbacks such as crystal aggregation, contamination.

Besides, in a research $NOBF_4$ was introduced as removing of surface ligands of NCs [31]. Positively charged and stable dispersed NCs were obtained. The applicability of $NOBF_4$ is limited since its oxidative and acidity ion level characteristics [29].

1.2 Quantum Mechanics

Understanding the photophysical properties of QDs provides a comprehensive approach about the energy states, electron hole pair generation, and quantum confinement related semiconductor nanocrystals issues. In this part, introduction will be done with material types and basic concepts about QDs and zero dimensional quantum confinement.

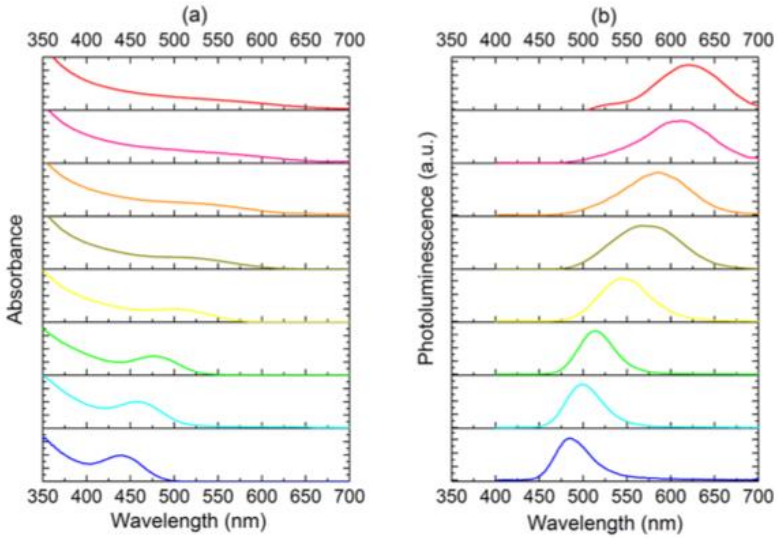

Figure 1.2.1 Absorption and emission spectra of InP/ZnS QD in different sizes [32]

These inorganic nanoparticles exhibit broad absorption spectra like bulk nanocrystals. Furthermore narrow and high capacity fluorescence efficiency is similar to molecular dyes. Tunability of optical properties is controlled by the size of QDs. Space between energy levels decreases as the QD size increases. Emission spectra is determined on the order of 1 eV [33]. These unique properties boosted up the potential usage of QDs in optoelectronic applications.

1.2.1 Quantum Dot Energy States

Two aspects as molecule like- and bulk crystal like- conduct to understand the approach of quantum dot energy states. In the *bottom-up* perspective, ordered individual atoms construct the core of QD. With the improvements in computational based area, this approach achieved a great importance by providing calculations on QDs [34].

Besides, *top-down* approach explains the contribution of finite sized QDs to characteristics of larger particles. Similarities of this perspective with quantum mechanical models serve as to understood well of fundamentals of QD photophysics.

In *top-down* approach, optical and electronic framework of QD is modeled based on bulky crystal properties [24]. Accordingly, it is essential to understand well of atomic orbitals in bulk structure in terms of energy state distribution (Figure 1.2.1.1).

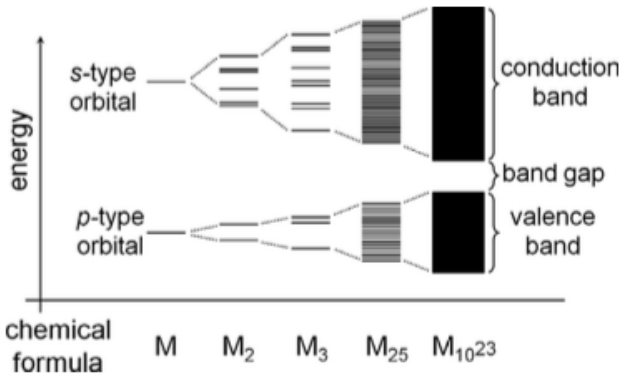

Figure 1.2.1.1 Increasing energy levels between bands as the number of atom in material decreases. Lost of discrete energy levels in bulky species and only continuous band observation [9]

Conduction and valence bands are formed by the lowest and highest unoccupied energy levels. Bands separation is provided by a specific gap known as band gap E_g which comprise no energy state, therefore, discrimination of bands is promoted. In the ground state, valence band loaded with electron is exposed to an outcoming energy. If energy is equal or greater than band gap, electron in valence band moves up to conduction band. This process gives rise to production of two charge carriers. In conduction band, negatively charged electron (e^-) is formed as positively charged hole (h^+) in valence band.

Dispersion curve of bulk semiconductor in Figure 1.2.1.2 explains the energy levels in terms of wavevectors.

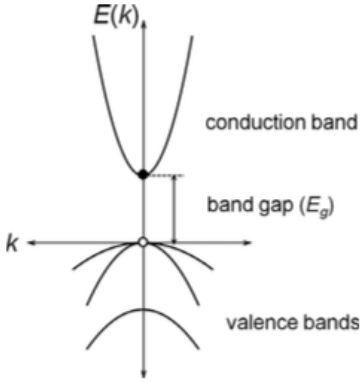

Figure 1.2.1.2 Energy band levels as k^2 and curves belong to bands are related to effective mass of e^- and h^+. Band gap (E_g) allows no energy states [9]

$$E_c = \frac{\hbar^2 k^2}{2m_c^*} + E_g \qquad (1.2.1\text{-}1)$$

Free movement of e^- and h^+ is summarized and characterized by a formula above ($p = \hbar k$, p as momentum, $\hbar$ as reduced Plank's constant, k as wave vector. Free particle energy is defined as $E = p^2/2m$ where m is particle mass). m_c refers to conduction band mass.

Contrary to continuous energy levels of bulky materials, reduced size of QD around band edges generates discrete energy levels. Density of states are defined as ρ, dimensionality as *d.* Zero dimension problem of QD is solved by delta functions.

$$\rho(E) \propto E^{\frac{(d-2)}{2}}, \qquad d = 1, 2, 3 \qquad (1.2.1\text{-}2)$$

Quantum confinement effect is not substantial for all semiconductor nanocrystals, merely become essential in case of QD size border on electron and hole's length level. This level (a_B) also called as Bohr radius refers to e^- Bohr radius in H atom. Counting radius of H atom as a_0, dielectric constant as ε, carrier effective mass as m^*, formula is given as:

$$a_B = \varepsilon \frac{m_0}{m^*} a_0 \tag{1.2.1-3}$$

Moreover, confinement of electron and hole together give in a new term exciton. It's Bohr radius is calculated as:

$$m_{exc}^{*-1} = m_e^{*-1} + m_h^{*-1} \tag{1.2.1-4}$$

Table 1.2.1.1 Bulk semiconductor properties [35]

		E_g (eV)	m_e^*/m_0	m_h^*/m_0		Electron a_B (nm)	Hole a_B (nm)	Exciton a_B (nm)
II–VI	CdS	2.48	0.25	0.6	5	1	<1	2
	CdSe	1.73	0.12	0.9[a]	6	3	1[a]	4
	CdTe	1.48	0.09	0.8[a]	7	4	1[a]	5
III–V	InP	1.34	0.073	0.45[a]	11	7	1	8
	InAs	0.35	0.023	0.57[a]	12	27	2	29
	InSb	0.17	0.012	0.44[a]	16	59	2	61
IV–VI	PbS[c]	0.42	0.087[b]	0.083[b]	17	10	11	21
	PbSe[c]	0.28	0.047[b]	0.041[b]	23	26	29	55
	PbTe[c]	0.31	0.034[b]	0.032[b]	33	56	48	104

[a] m_h^* listed for heavy hole.
[b] All data at 4 K and $m_{e,h}$ are calculated as $3\bar{m}^{-1} = m_{//}^{-1} + 2m_{\perp}^{-1}$.

Electron and hole diameter in 3 nm of PbSe QD could respond two times confinement energy than same sized CdSe QD. As shown in Table 1.2.1.1, electron Bohr radius is larger than holes. It could be concluded that quantum confinement effect in conduction band is more notable than in valence band.

1.2.2 Experimental proofs describing the quantum confinement effect

Absorbance measurement is a kind of technique to detect different sized QDs. These semiconductor nanocrystals are excited with a stimulator between the ranges of 300-700 nm and give particular picks in response to size of crystals in discrete wavelengths.

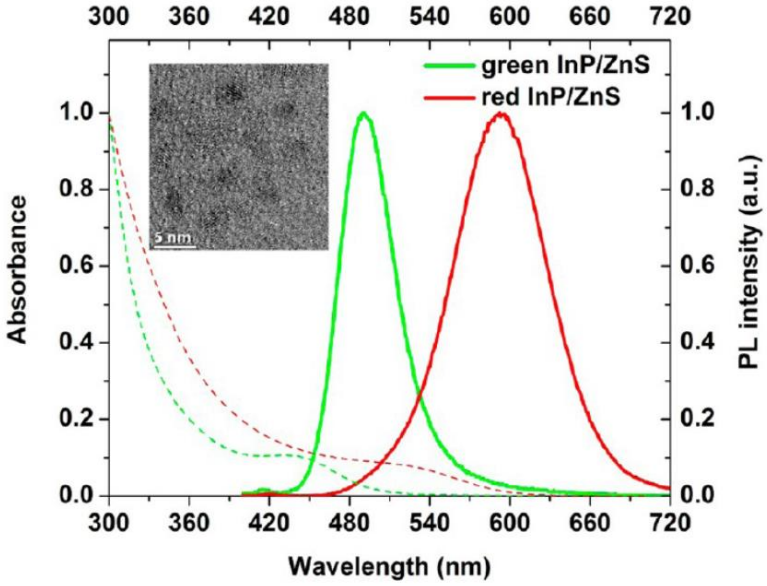

Figure 1.2.2.1 a) Absorbance (dashed line) and emission (solid line) spectra of green and red fluorescence emitting InP/ZnS QDs [36]

Highly monodisperse QDs could be detected by the absorption and emission spectra. Narrow full width at half maximum (FWHM) value in PL emission spectra demonstrate highly monodisperse QDs. PL of core quantum yield (QY) is calculated in a range 10-50% by comparing with a reference sample QY. Post modification such as adding capping agents or shell could promote the efficiency [37], [38]. From experimental point of view, there is a restriction part in absorbance spectroscopy on detection of multiple transitions due to QD energy gaps. Prevailing on this problem, techniques as photoluminescence excitation (PLE) were introduced [39].At a fixed emission value, excitation wavelength is scanned. Other strategy is using fluorescence line narrowing (FLN) spectroscopy [40]. FLN instrument is capable of exciting smallest sized QDs.

Optimization of colloidal QDs properties include epitaxial growth of a second layer called as shell on top of the presynthesized core particle. Surface atom passivation is provided by inorganic materials due to high ratio of surface to core atoms. Delocalized electrons and holes in the core of nanocrystal are capable of locate on energetically trap charge carriers because of defective passivation by organic materials.

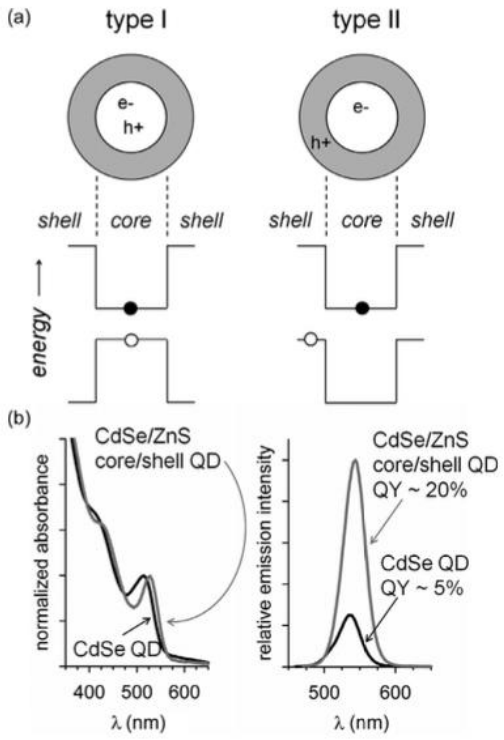

Figure 1.2.2.2 a) Band alignment in type I and type II core/shell QDs. Electron and hole confinement preserved in type I core QD; one of the carrier remains in core, other one localized in the shell structure. b) Absorbance & emission spectra difference between core QD and core/shell QD (type I) Red shifted absorbance value of core/shell QD occurs since the exciton wavefunction penetration into the shell. Emission capacity of core/shell QD is 4X of core QD due to defections on the surface of core QD [9]

Classification of core shell QDs depends on their band energy comparison in core and shell, for instance in type I the conduction band energy is lower in the shell than in core one. In type II, it's vice versa. Alignment between core and shell affects the photoexcited electrons and holes; while photoexcited electrons quickly relax to their minimum conduction band states, photoexcited hole relaxation occurs toward the maximum valence band state (Figure 1.2.2.2). CdSe/ZnS QD (type I) is constructed by a thin shell layer of ZnS with a bulk bandgap of 3.6 eV [41]. Finite potential difference between core and shell is approximately 1 eV which diminishes the penetration of exciton wavefunction into the shell. Moreover surface passivation provided by core/shell/shell QD increase the PL intensity up to 5-10 fold [41]. A reported PL intensity 80% [42] with high brightness and surface protection make use of these type of QDs in biological applications [2]. Most studies base on cadmium chalcogenide materials which is relatively simple to synthesize with great optical quality [6]. By

virtue of highly toxic characteristics, massive amount usage of material containing cadmium in technological area and toxicity level in vivo applications conducted researchers to investigate new materials with reduced toxicity with cost efficient productions. The concern shifted to Cd-free alternatives particularly InP QDs [43]. Cd-free synthesis depends on phosphorus precursor $(TMS_3)P$ [44], PCI_3[45], P_4, [46] Trioctylphosphine (TOP) [47]. Widely used $(TMS_3)P$ in optimized protocols give QDs with 40-60 FWHM but its higly toxic gas (non-environmental) and expensive price properties make large scale synthesis difficult [15]. $(DMA_3)P$ as an alternative phosphorous precursor (relatively safer and cheaper) used to produce QDs with several combinations of InP/Zn- QDs (P:DMA dimethlyamino, DEA diethylamino; InX as InCI, InBr, InI; ZnS and ZnSe) [48]

1.3 Experimental

1.3.1 Materials

InP/ZnS (contains TMSP): Indium(III) acetate (99.99%), myristic acid (99%), 1-octadecene (90 %), 1-dodecanethiol (98%), zinc stearate (purum), tris (trimethylesilyl) phosphine (95%) were purchased from Sigma Aldrich.

InP/ZnS (contains TOP): Indium(III) chloride (99.999 %), indium(III) bromide (99.999 %), indium(III) iodide (99.998 %), zinc(II) chloride (99.999 %), tris(dimethylamino)phosphine (97 %), and zinc stearate (technical grade), oleylamine (80-90 %), trioctylphosphine (97 %), Octadecene (technical 90 %), mercaptosuccinic acid, ammonium hydroxide, TEOS, APTES and sulfur powder were purchased from Sigma Aldrich.

Organic and other solvents: Absolute ethanol , acetone (99.5%), methanol (99.8) and hexane (95%) were purchased from Merck.

1.3.2 Characterization Techniques

QD synthesis was done under vacuum/argon gase based manifold system. Absorbance

and photoluminescence spectrum results were recorded on Genesys 10S UV-Vis Spectrometer (Mutlugun Lab) and Cary Eclipse Fluorescence Spectroscopy (Mutlugun Lab) respectively. Photoluminescent quantum yield (PLQY) was calculated by formula given below:

$$\Phi_{\text{flu}}^{\text{sample}} = \Phi_{\text{flu}}^{\text{reference}} \left(\frac{F^{\text{sample}}}{F^{\text{reference}}} \right) \left(\frac{\eta^{\text{sample}}}{\eta^{\text{reference}}} \right) \left(\frac{\text{Abs}^{\text{reference}}}{\text{Abs}^{\text{sample}}} \right) \quad \textbf{(1.3.2-1)}$$

QY for all fluorescent samples was calculated as in equation above. (Φ: Quantum yield, F: integrated emission area, η: refractive index o solvent, Abs: absorbance value of selected wavelength) [49] Rhodamine 6G (QY: 95%), sulforhodamine (QY:90%) dissolved in absolute ethanol were used as reference to determine the QY of samples. All optical densities at particular wavelengths were retain below 0.1 to prevent internal filtering effects.

Time resolved photoluminescence spectroscopy (Picoquant Fluotime 200-AGU) was used to measure life time of particular samples. 10000 photon count was completed to plot the time line of particular sample. Maximum emission values of samples at 450 nm taken from PL specrophotometry were entered. To analyse fluorescence decay, Fluofit software was utilized. Transmission electron microscope (TEM) and scanning electron microscope (NanoSEM) -BILKENT UNAM- were used to determine the surface and structural analysis of samples. While magnification with SEM allows to observe object at micron level, more detailed results at nanometer scale could be illustrated by TEM.

Dimpling and ion milling processes are integral part of TEM specimen preparation. Diluted samples are dropped onto grids and pilko tab hold the grid in proper position. After drying of sample solution in an hour, grid is placed into TEM component and analysis starts. SEM specimen preparation is needed an extra step before analysis. Non-dense material composition generates too low signal for surface scanning images. Therefore, an extra coating with gold provides a strong signal to visualise depth with 3D appearance. QD samples were dropped onto pin mount stand and waited for drying for an hour. Then, samples on the pin was coated with gold and observed with SEM.

Hydrodynamic size distribution of nanocrystals were recorded by Malvern Zetasizer. This instrument measures size of particle in nanometer scale. Proper dilution level is essential to acquire good results because of colloidal QD particle size is nearly picometer scale. Polydispersed particles or aggregated ones have potential to change the precision of measurement.

1.3.3 Synthesis Procedure

Alloyed-Core synthesis of InP/ZnS QD (contains TMSP)-1X volume

0.1 mmol $InAc_3$ and 0.3 mmol MA were mixed with 8 ml ODE in triple neck flask. Under vacuum, the solution was stirred for 1 hour at 95 °C. To obtain a clear solution, mixture was kept going to stirred at 120 °C under Ar gas for 20 min. After cooled down to 25 °C, 0.1 mmol zinc stearate and 0.1 mmol dodecanethiol were added into clear solution and on the back of heating up the mixture to 230 °C under gas, 0.1 mmol TMSP in 1 ml ODE was quicly injected into solution. Following increasing temperature to 285 °C , alloyed-core QDs were generated at 285 °C after waiting for 10 min and then cooled down to 25 °C.

Shell synthesis of InP/ZnS QD (contains TMSP)-1X volume

For shell coating, 0.2 mmol zinc stearate was added into solution at 25 °C and heating up temperature to 230 °C under gas started the passivation and growth of shell on top of alloyed core. After 2 hours, 0.4 mmol dodecanethiol in 1 ml ODE was injected into mixture. The synthesis was completed with 1 hour wait at 230 °C and solution was cooled down to 25 °C. (QD cleaning was described in detail under the cleaning procedure title)

(2x volume of QDs core synthesis: 0.2 mmol $InAc_3$, 0.6 mmol MA, 0.6 mmol zinc stearate, 0.2 mmol DDT, 0.125 mmol TMSP/ shell: 0.4 mmol zinc stearate, 0.8 mmol DDT)

(5x volume of QDs core synthesis: 0.6 mmol $InAc_3$, 1.8 mmol MA, 20 ml ODE, 2 mmol zinc stearate,0.25 mmol DDT, 0.125 mmol TMSP/ shell: 1 mmol zinc stearate, 2 mmol DDT)

Core synthesis of red fluorescence light emitting InP QDs (contains TOP):

QD synthesis method was modified from the article of Tessier et al [48]. 0.45 mmol $InCI_3$ and 2.2 mmol $ZnCI_2$ were mixed with 6 ml oleylamine solvent in triple neck flask. Under vacuum, the mixture was stirred at 120 °C for 1 hour. Then, under inert atmosphere, the system heated up to 180 °C. Upon reaching to specified temperature, 250 µl tris(dimethylamino)phosphine was quickly injected into solution. Allied with the phosphorous precursor injection for 20 min at 180 °C, core stage of nanoparticles accomplished (main solution).

Core synthesis of orange fluorescence light emitting InP QDs (contains TOP):

Same protocol was followed for the synthesis of orange light emitting QDs except 0.45 mmol indium(III) bromide substituded for indium(III) chloride.

Core synthesis of green fluorescence light emitting InP QDs (contains TOP):

Same protocol was followed for the synthesis of green light emitting QDs except 0.90 mmol indium(III) iodide substituded for indium(III) chloride.

Shell synthesis of InP QD (contains TOP)

After achieving core structured nanocrystals as outlined above, passivative and protective layer called as shell was sythesized onto core nanocrystals. Primarily, 2.2 M stock solution (0.72 g Sulfur in 10 ml TOP) was prepared in glovebox. 1ml TOP-S taken form stock solution was slowly added into triple neck and at 40 minutes the system was heated up to 200 °C. At 60 minutes, readily prepared 4 ml Zn-Stearate/ODE (2g Zn-Ste in 7 ml ODE in triple neck under Ar gas at 170 °C) was injected into main solution containing core QDs and the temperature heated up to 220 °C. At 90 minutes, 1ml TOP-S at 240 °C was injected into colloidal solution. At 110 minutes, 2 ml Zn-Ste/ODE was added at 260 °C. At 130 minutes, 0.7 ml TOP-S (2.2 M) was slowly loaded at 280 °C for 20 min. At 150 minutes, 2 ml Zn-Ste/ODE was injected and after 15 min the system was cooled down to room temperature.

1.3.4 Cleaning procedure& Phase transfer

Properly synthesized QDs were cleaned with a process to remove excess ligands on the surface of QD. At first, QDs in triple neck were transferred to a falcon and half volume

of hexane organic solvent was added, vortexed for 1 min and centrifuged at 5000 rpm 15 min. Supernatant (stock solution) was transferred to another falcon. This step was repeated to discard unreacted (pellet) chemicals from QD solution. To remove excess ligand, acetone as double in volume was added into stock solution and centrifuged at 5000 rpm for 5 min. After removing liquid, pellet including QD in precipitate form could be seen obviously. This part is the general cleaning procedure. Following steps were performed for InP/ZnS (contains TOP). Afterwards, pellet QDs dried at room temperature (overnight) was weighted (0.25 g) and a second washing treatment was done to prepare QDs for phase transfer.

Most of organic ligand removing makes attachment of water based ligand easier. For second washing, acetone washing process was repeated. After centrifugation, pellet QDs were dissolved in 10 ml hexane and put into 100 ml glass bottle. 15 ml ammonium hydroxide and 40 ml water also added into solution and mixture was stirred on hot plate at room temperature for 3 hours. Then, 0.75 g MSA was put into mixture and overnight stirring helped to attach the MSA onto QD surface. In case of no passage to water phase of some QDs (WQD), these ones could be washed with acetone and mixed with MSA again. For precipitation of water based QDs, ethanol is added into mixture -QD:ethanol 4:1 (v/v)- 5000 rpm for 10 min was sufficient to precipitate aqueous QDs which are then dissolved in water for further application.

1.3.5 Polymeric films

Polymer 1g PMMA was dissolved in 10 ml anisole or toluene (10% w/v). Mixture was stirred overnight at 50 °C to obtain a clear polymer solution. Then QDs prepared in toluene were added into polymer for mixing (2 hour). At the end, QD polymers were dropped onto clear glass surface.

1.4 RESULTS AND DISCUSSIONS

InP/ZnS (containing TMSP) synthesis procedure was used to achieve highly efficient alloy shell semiconductor nanocrystals with low FWHM. Figure 1.4.1 shows the alloy/shell QDs after hot injection synthesis.

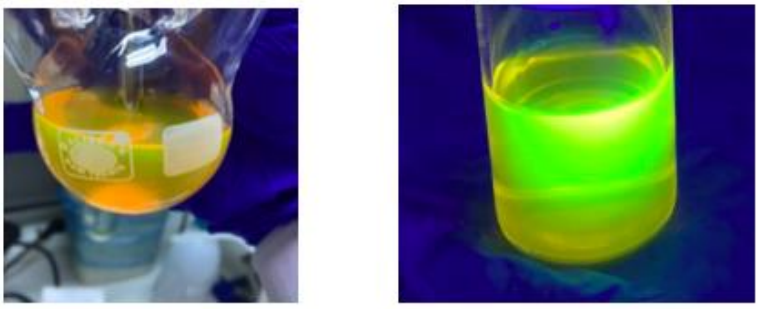

Figure 1.4.1 InP/ZnS QDs in triple neck and in vial a. before cleaning b. after shortage of ligands with acetone

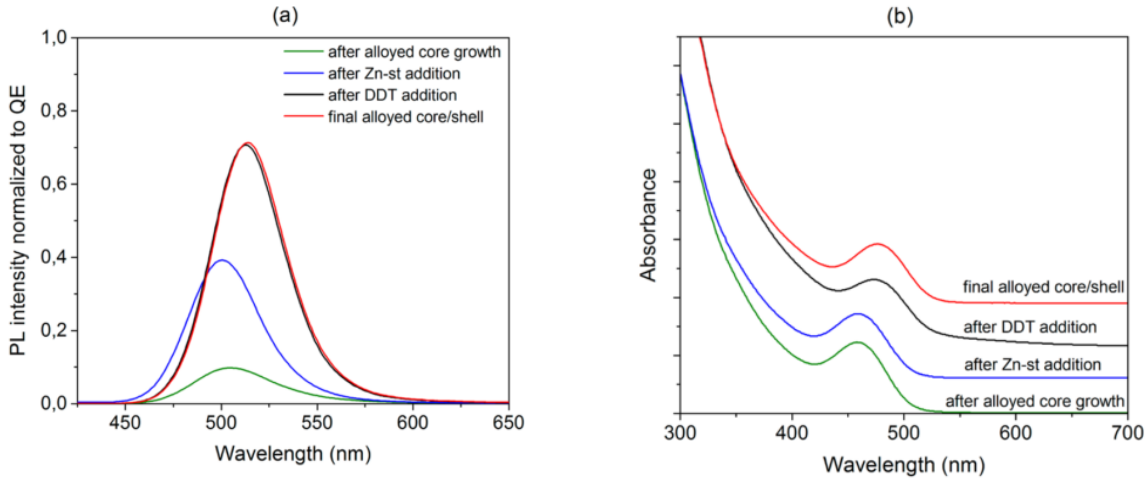

Figure 1.4.2 Figure InP/ZnS QDs (containing TMSP) during formation of nanocrystals a. PL spectra b. absorption spectra

Distinctive characteristics of alloyed core QDs are related to their alloyed structure. Precursors (Indium and myristic acid) and shell materials (zinc stearate and DDT) were fused simultaneously to generate alloyed core framework. This arrangement of alloyed core/shell QDs allowed high surface passivation of nanocrystals due to zinc stearate and low FWHM relevant to DDT. PL intensity of alloyed core is lower compared to alloyed core/shell QDs. Furthermore, shell capping shifts the emission wavelength to red side due to size increment capability of zinc stearate. Absorbance spectra (peak point) also shift toward red side (Figure 1.4.2).

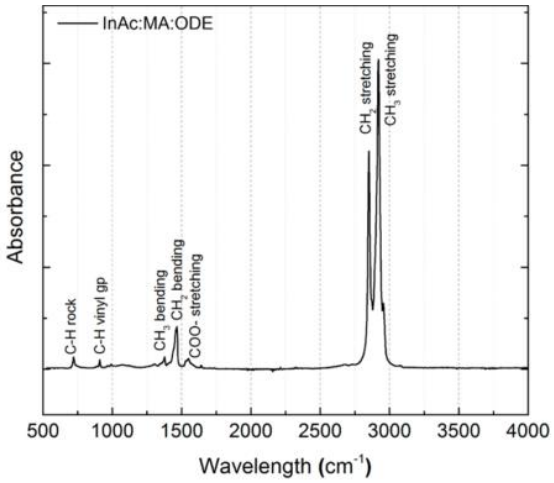

Figure 1.4.3 FTIR spectrum of InP/ZnS QDs including myristic acid and ODE

The bands at 2800 and 2920 cm^{-1} refer to CH_3 and CH_2 stretching bonds respectively. Vinyl group at 900 cm^{-1} and CH rock bonds at 730 cm^{-1} demonstrate the formation of QDs with myristic acid and DDT ligands (Figure 1.4.3).

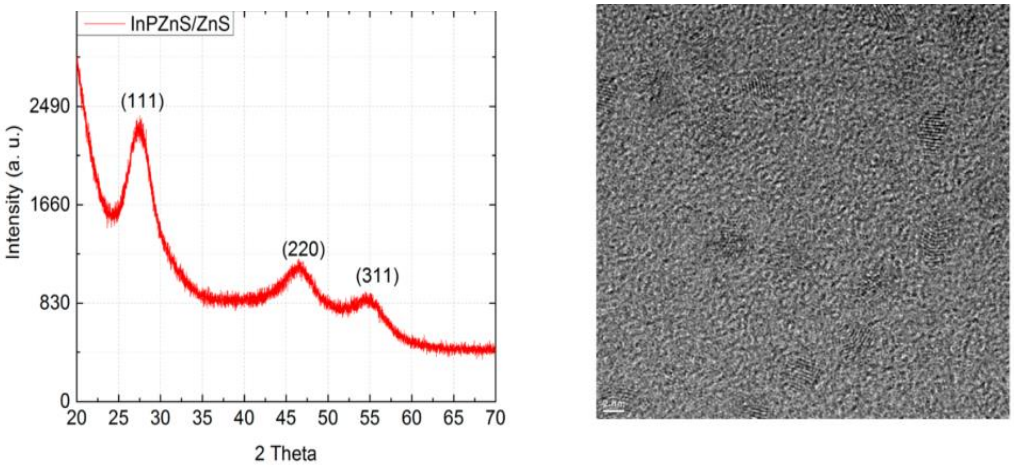

Figure 1.4.4 InP/ZnS QDs characterization a.XRD spectrum b. TEM image (scale bar 2 nm)

X-Ray diffraction (XRD) determines the structure of sample crystalline. Peaks shown in figure refer to cubic zinc blende pattern. TEM also showed the size of QDs around 3.5 nm (Figure 1.4.4).

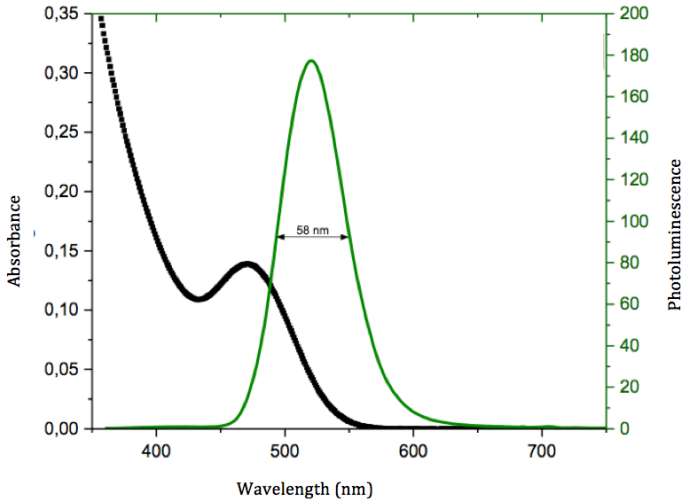

Figure 1.4.5 PL and absorption spectrum of InP/ZnS QDs

Scale up synthesis of InP/ZnS QDs was done to obtain high amount of QD at the same time. As seen in Table 1.4.1 1x and 2x volumes have the same FWHM but 5x volume has lower FWHM. PLQY for all fully synthesized samples were range over 85. As expected, PLQY of 5X volume-core is lower than alloyed core/shell QDs. 10 nm emission shifting was a result of shell capping.

Table 1.4.1 Table Scale up synthesis of InP/ZnS QD (containing TMSP) and their characterizations (Emission wavelength, FWHM and QY)

Sample	Emission (nm)	FWHM (nm)	PLQY
1x volume	528	54	88
2x volume	511	54	96
5x volume (only core)	498	49	76
5x volume (core+shell)	508	50	87

InP/ZnS QDs (including TOP)

As mentioned in the experimental part, core generation is provided by $InCI_3$ and $ZnCI_2$ precursors. Oleylamine contributed to synthesis as solvent and ligand, which facilitate to reaching relatively high temperature (340 °C) for shell formation properly. Size dispersity of nanocrystals is controlled and decreased by $ZnCI_2$. Although precursors

listed above are needed, $(DMA)_3P$ as phosphor source relatively occupy the crucial role for core development. Low price and toxicity compared to TMSP like phosphorus sources arouse interest for this chemical.

Shell development is maintained by sulphur dissolved in TOP (TOP-S). As an alternative to dodecanethiol, TOP-S does not stimulate blue shifted emission. Each addition of TOP-S and $ZnCl_2$ into the synthesis mixture following the rise of temperature provides a protection of oxidation layer of InP QDs. Formation of shell layer onto core structure of QD increase the diameter of nanocrytals which shift the emmision wavelength. Possible explanation for this event is the lattice mismatch of InP and ZnS. In addition to low price (total synthesis), other key point is the chemical yield. The alteration of P:InX_3 ratio from 1:1 to 3.6:1 boosted up the chemical yield from 30% to 85%.

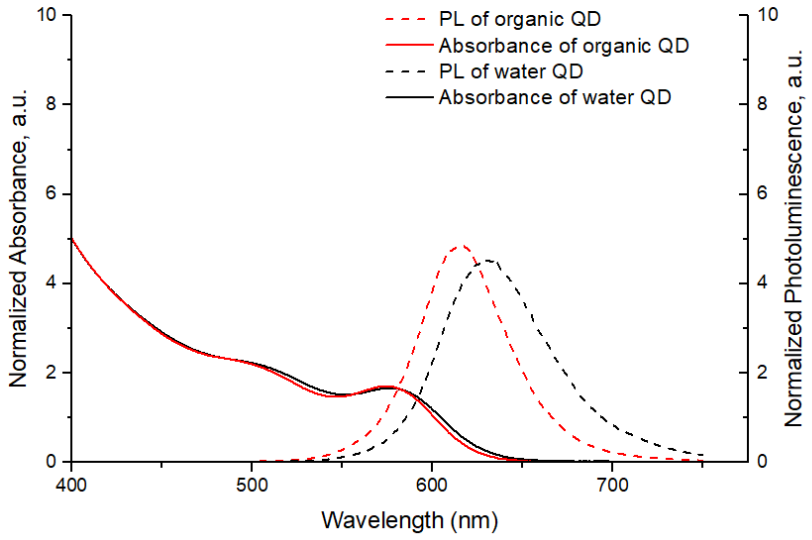

Figure 1.4.6 Absorption and emission spectra of organic and water based InP/ZnS QDs

As seen in Figure 1.4.6, organic InP/ZnS QDs have lower FWHM and higher PLQY compared to aqueous QDs. Shifting of emssion wavelentgh of aqueous QD is caused by phase transfer in which MSA attached to QDs after removing most of TOP-S ones. This alteration also affected QY negatively due to incomplete surface passivation capacity of MSA. Dimension of QD in hexane and water was 6.38 nm and 5.21 respectively (Figure 1.4.7).

a.

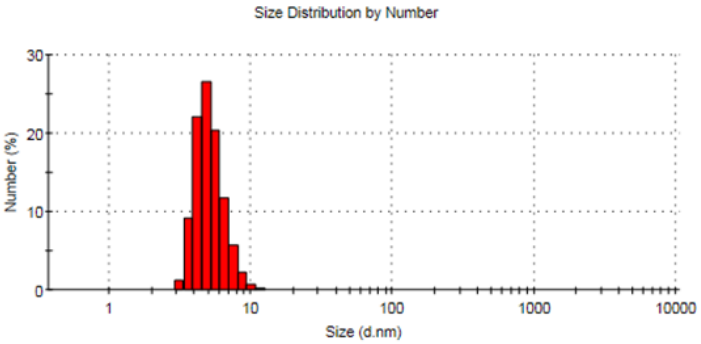

b.

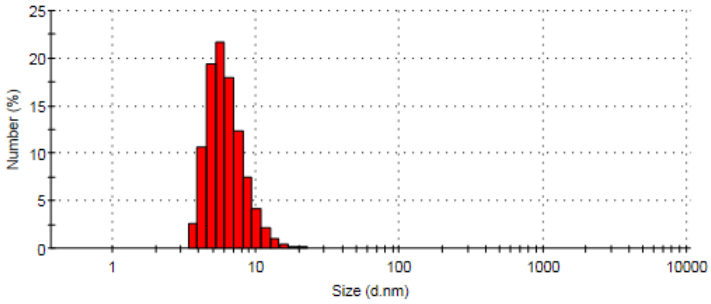

Figure 1.4.7 Size distribution by number of QD a. organic b. water based QD

Figure 1.4.8 shows the vibration peaks of organic QDs functionalized with C-H (stretch bond) groups at 2820 cm^{-1} and C-C groups at 3223 cm^{-1}.Furthermore, the stretch bands at 1620 cm^{-1}, 1457 cm^{-1} refers to C=C vibrational ,C-C stretching bands (vinyl group) respectively. Functional groups mentioned above indicates the presence of TOP ligands for organic QDs. Aquoeus QD spectra with ligand MSA includes carboxylic and sulphur related group. O-H, S-H stretch bonds at 3326, 2551 cm^{-1} and C=O, C-O, C-S stretch band at 1553, 1377, 715 cm^{-1} respectively are associated with the successful ligand exchange procedure.

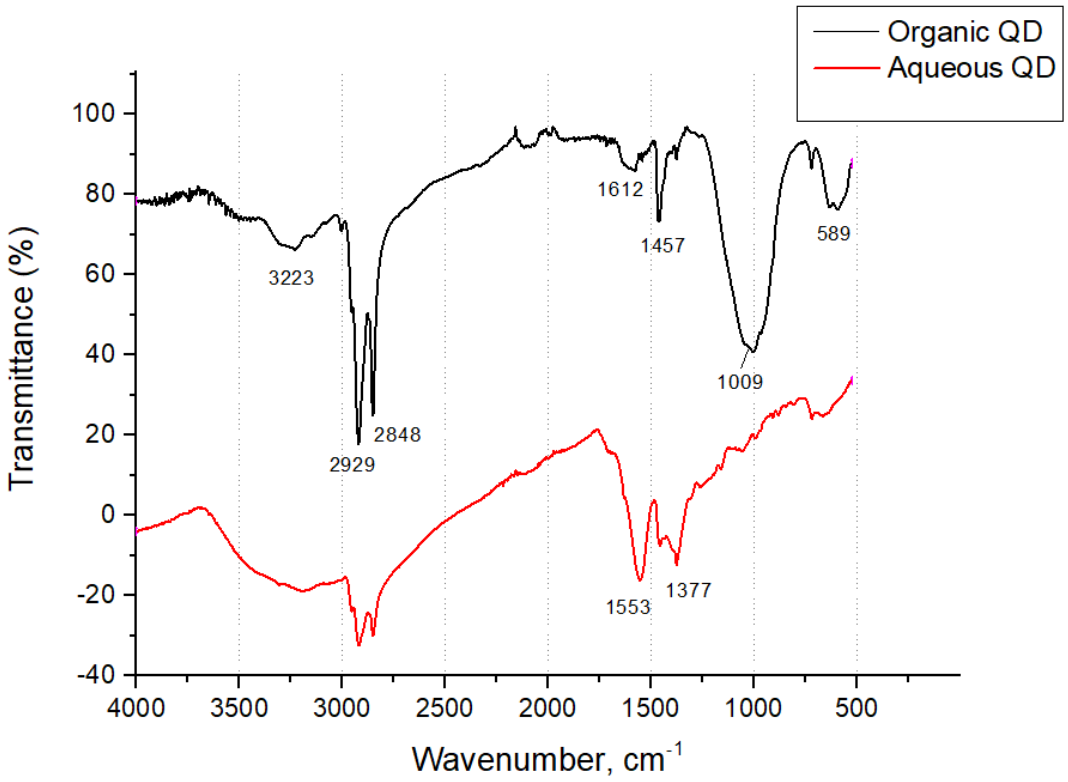

Figure 1.4.8 FTIR analysis of organic and water based QDs

QD emitting at different wavelengths was obtained by size tuning property of these nanocrystals. By altering In halide precursor (InX; X:CI, Br, I) emission wavelengths were measured at 530, 590, 620 roughly. Shifting emission to less than 500 or more than 630 is restricted by precursor solubility in oleylamine (Figure 1.4.9).

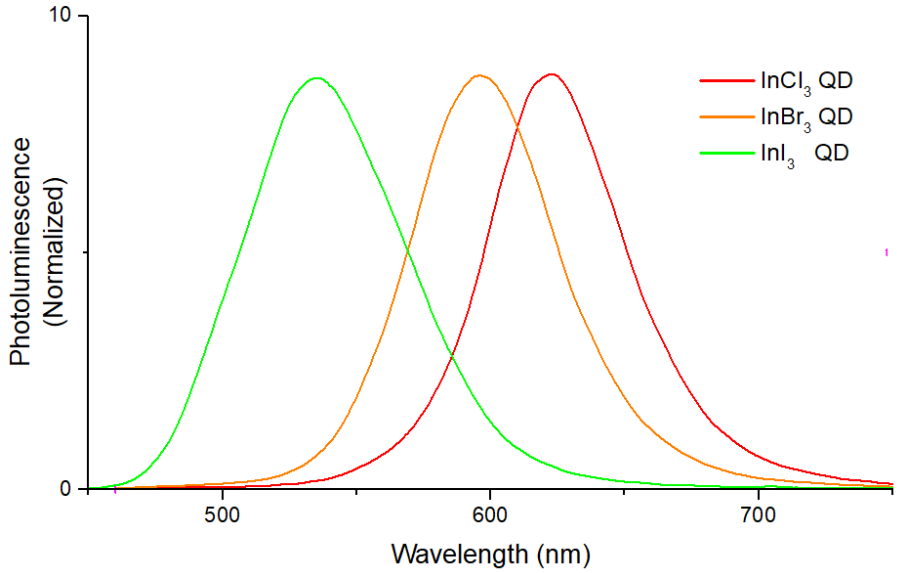

Figure 1.4.9 Halide effect on PL spectra of QDs

PDMA as phosphor precursor was injected into synthesis solution in different concentrations. Best FWHM and PLQY were obtained by using 250 ul PDMA. Concentration changes also affected the emission wavelength of QDs (Figure 1.4.10).

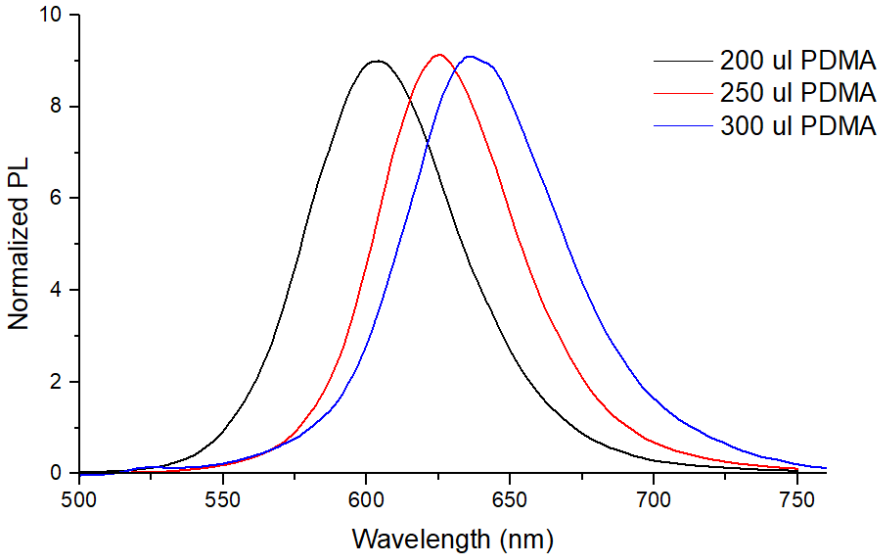

Figure 1.4.10 PDMA effect on PL spectra of QDs

Time resolved spectroscopy analyses the excited photon time delay of samples. The delay times are plotted according to occurrence of emission throughout the time following excitation process. As seen in graphic, aqueous QDs have a bit different line compared to organic QDs. According to table, there are three components of each of plotted line. Percentages of component 1 (T1) demonstrate the difference between organic and water based QD 20.60% and 25.56% respectively. T2 and T3 also indicate the alteration of component percentages due to phase transfer (ligand alteration). Average time relapse is the same for both of the samples.

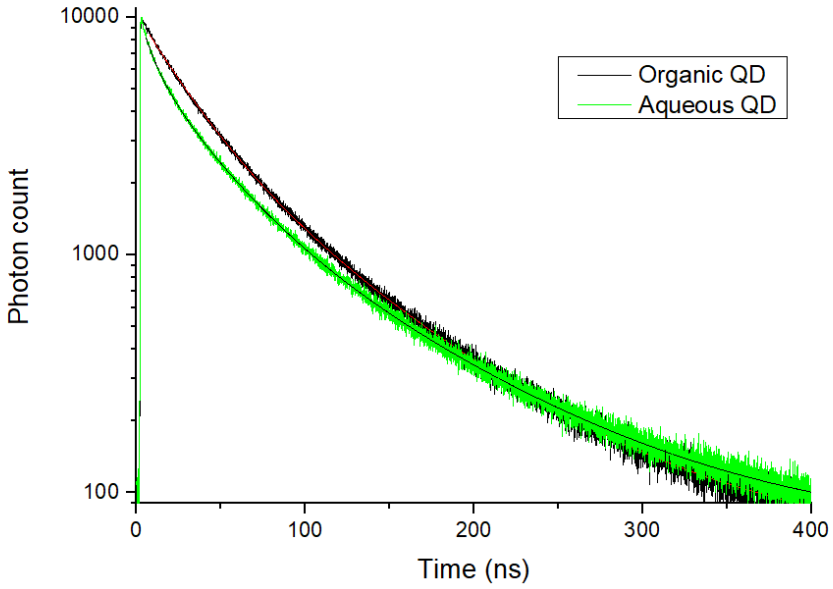

Figure 1.4.11 Time resolved spectra of organic and aqueous quantum dots

Table 1.4.2 The lifetime components of organic and aqueous quantum dots

Sample	A1	T1 (ns)	A2	T2 (ns)	A3	T3 (ns)	Tavg
Organic QD	1909.3 ± 20.3	94.760 ±0.665 **20.60%**	5688.7 ±51.4	32.677 ±0.405 **61.38%**	1670 ±102	14.65 ±1.04 **18.02%**	42.218
Aqueous QD	2053.6 ±19.9	94.760 ±0.665 **25.56%**	4109.9 ±52.6	32.677 ±0.405 **51.15%**	1871 ±132	8.062 ±0.696 **23.29%**	42.813

Organic and aqueous QDs were also compared according to their emission time capacity (TRPL). As demonstrated in Table 1.4.2, life time of both samples have three components in which the percentages of each of them differs. Organic QDs T1,T2 and T3 values were recorded as 20.60, 61.38, 18.02 % respectively. On the contrary, percentages in aqueous QDs was seen as 25.56, 51.15, 23.29 %. Despite similar average T values, changes in life time components showed the difference between organic and aqueous QDs.

Polymeric films

Properly embedded QDs into polymeric films is essential in display technology, biosensor applications. In this part, it was studied on dissolving QDs in particular polymers and preventing the decrease of QY after embedding.

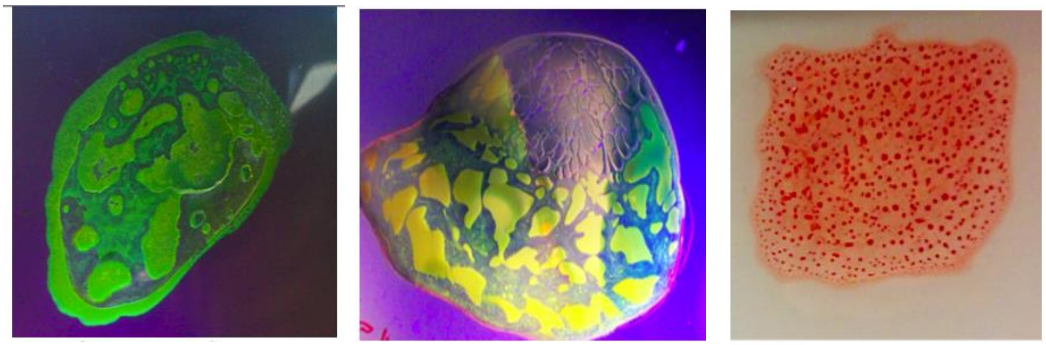

Figure 1.4.12 a. Green emitting InP/ZnS QDs in PMMA-anisole polymer (10% w/v) b. green and red emitting InP/ZnS QDs in PMMA-anisole polymer (10% w/v) c. red emitting InP/ZnS QDs PMMA-toluene polymer (10% w/v)

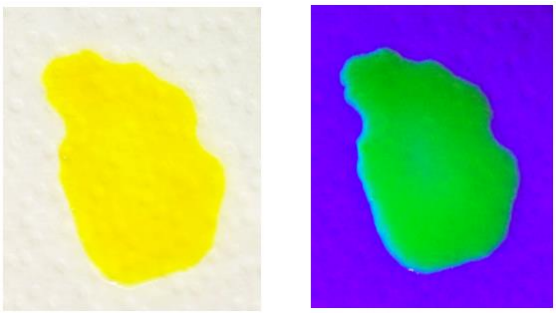

Figure 1.4.13 InP/ZnS QDs PMMA-toluene a. films under normal light and b. UV light (5% w/v)

PMMA polymer was dissolved in toluene and anisole to detect the best solvent for QDs. However, green QDs did not dried in PMMA film.

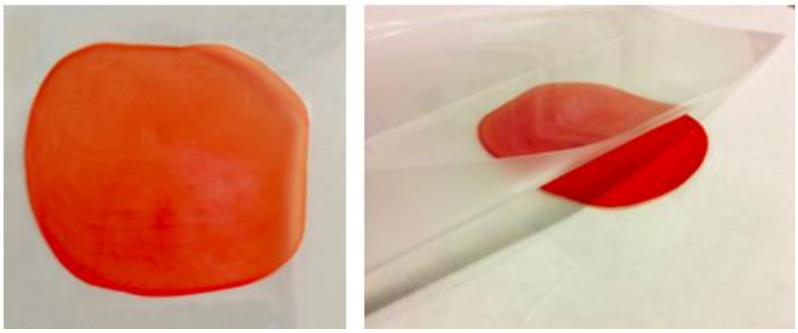

Figure 1.4.14 Red emitting InP/ZnS QDs PMMA-anisole polymer (10% w/v)

Red emitting QDs were sythesized with TOP ligand which allowed QDs better drying capability but PMMA-toluene polymeric film was not suitable for embedding procedure. Therefore, red emitting InP/ZnS QDs were dissolved in PMMA-anisole polymer and as seen in figure 1.4.14 laminated QDs barely losed the QY (18% reduction). FWHM value was even stable after lamination.

Chapter 2

Biodetection

2.1 Aqueous based semiconductor nanocrytals

Initiated from 1980s by great effort of studies [47] [48], aqueous synthesis of colloidal QDs has drawn attention over three decades [52] [53] [54]. CdS QDs were firstly perfect model to understand the size dependent optical characteristics of colloidal nanocrytals. This routes shifted to the synthesis of other types nanocrytals such as zinc, cadmium, mercury [55] [56]. The critical phenomena, quantum confinement effect, triggered the detailed discovery of the colloidal NC applications in biomedical 39 and optoelectronic scopes [30].

Nonaqueous hot injection' method developed by researchers [57] [58] [59] gave rise to highly florescence efficient and structurally uniformed QDs. High temperature organic synthesis approach derives lower defects and enable to several ligand selection [60] [61].

Ligand transfer facility of these QDs serve as attachment of biomolecules in order to detect the microorganisms by mineralization approach [62] [63] Furthermore, nucleic acid conducted QD synthesis approach is a robust method due to targeting of NCs with specific DNA and protein which are related to particular diseases [64], [65].

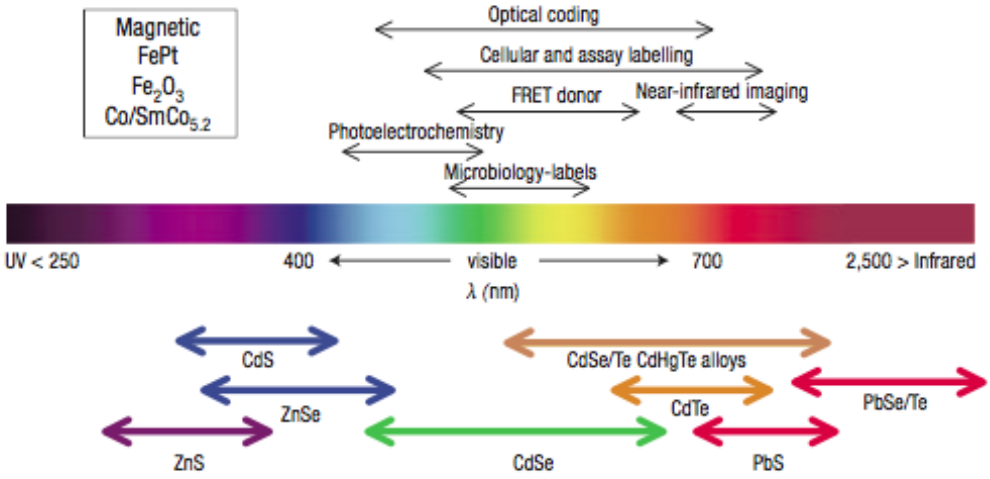

Figure 2.1.1 Illustration of QD core structure usage area in terms of emission wavelength. Biological interet is mostly focused on visible and near infrared regions [57]

In optoelectronic devices, long alkyl chains have very limited solubility in water. Therefore, aqueous based QDs with short ligand are preferred since diminishing dielectric barrier. TiO_2 like colloidal QDs containing ligand with mercapto acid and thiol derivates are favorable to produce thin dense films [53] [66]

A notable and stable water based NC synthesis was done by Rogach team by using mercaptoethanol ligand. Effective binding of thiol ligands onto surface of CdTe NCs formed the dots with 3 % QY 13. Other constituent achievements with high colloidal stability were done by thioglycolic acid (TGA) capping onto CdTe NCs with 18% QY [67]; mercaptopropionic acid (MPA) with 38% QY [68].

2.2 Inorganic & Biological Hybrids

Inorganic material and biomolecule combination provides particular spectral characteristics from nanoparticle and cellular attachment functionality from biomolecule. Finite size capability of QD allows simultaneous binding to various proteins. Acting as scaffold surface for protein, hybrid structure of nanocrystals with biomolecules construct multifunctional pattern [57]. Maltose binding proteins conjugates with 6 nm sized QD decrease the binding capacity to nanocrystals if their recognition site is lost [69].

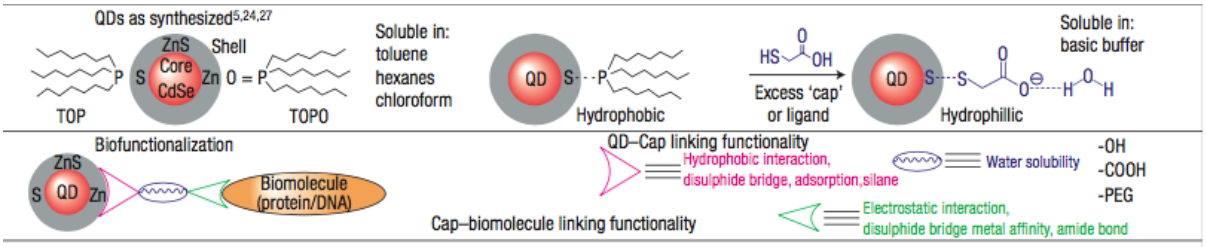

Figure 2.2.1 QD soluble form in organic and aqueous solutions by changing the capping molecule. Biofunctionalization of QDs that provides attachment site for protein and DNA [57]

Protein attachment can be classified in three main areas: EDC treatment of carboxy groups of QD to surface of amines; direct conjugation of QD to particular protein by thiol capped peptides; noncovalent interaction of QD by using engineered proteins. Poor QD stability in pH alteration of EDC applications causes unwanted intermediate accumulation. Capsulization of QD with a polymer shell could culminate in nonspecific binding of targeting molecule onto nanocrystal surface [57].

Direct attachment consists mainly on surface-protein interaction. A study carried by Weiss group inludes phytochelatin peptide covering of CdSe/ZnS QDs. This comprehensive study includes not only surface passivation and phase transfer, but also biochemical alteration [70],[71]

Other approach is related to adherence of biomolecules onto target surface. Positively charged engineered proteins self-accumulate onto surface of negatively charged QDs due to electrostatic interaction. This procedure is practical in different areas including protein G binding to IgG site of an antibody [72], nonspecific protein adsorption onto QDs [73].

2.3 Silica Nanospheres

QDs with fascinating optical characteristics have attracted large scale area such as nanosensors and bioimaging. However, II-VI semiconductor NCs could deteriorate and lose chemical stability due to harsh conditions (pH, oxygen, solution with metal ions, quenchers) [54]. To prevent unstable PL intensity of QDs, several ideas were put forward. Conjugation of QD with a fluorophore was studied [74] but fluorescence fluctuations caused many turmoil in quantitative analysis results. In addition cytotoxic heavy metal ion forestalled the utilization of QD in interested applications [54].

Therefore, appropriate techniques were investigated to overcome the PL and cytotoxicity problems such as polymer spheres [75] and silica dots [76]

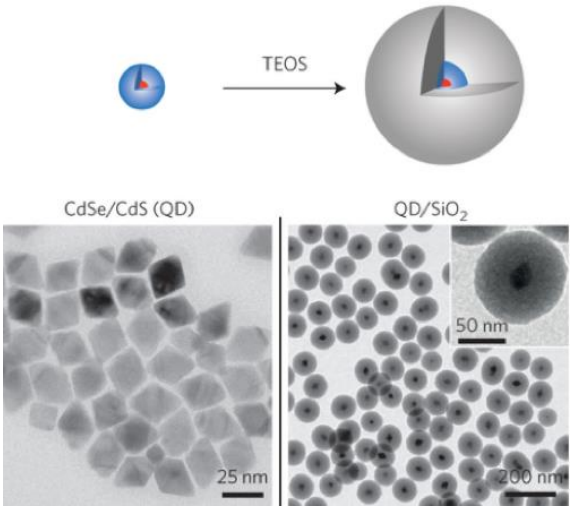

Figure 2.3.1 Schematic illustration of silica coating stages (top) and TEM images (bottom) a. Cd QD b. Quantum Dot/ SiO_2 nanoparticles [77]

Biocompatible, inert and aqueous solubility properties of silica dots intensified the researches into silica coating QDs [78]. On top of providing colloidal stability, diminishing cytotoxicity, silica shell enables functionalization of QD surface ligands. However, Stöber procedure and reverse microemulsion technique not only plunge the PL of QD, but also cannot maintain QD from harsh microenvironment [79]. Approximately 50% of initial CdTe QD PL is lost after $CdTe/SiO_2$ nanoparticles processed by reverse microemulsion technique [80]. Besides this kind of approaches, instability in harsh microenvironment problem could not solved.

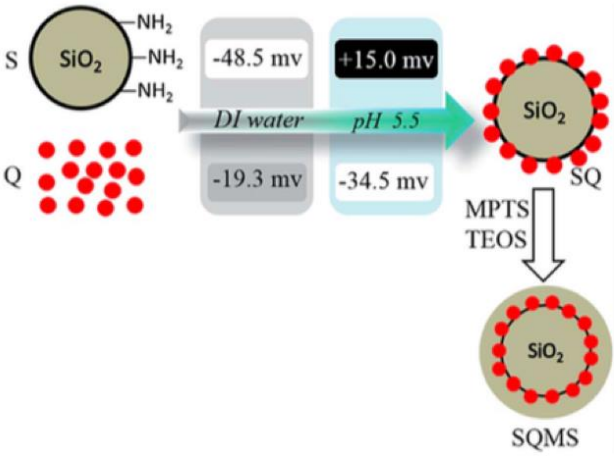

Figure 2.3.2 Electrostatic accumulation of MSA capped QDs onto amino functionalized SiO_2 [81]

A remarkable process (double silica coated) was applied by a group [81] This approach is called as sandwich model that SiO_2/CdTe QD/ SiO_2 composite structure was constructed respectively. Mercaptopropionic acid capped QDs with carboxylic group electrostatically attract amino-functionalized silica dots. Composite material preserves nearly 80% of initial QY of CdTe QD. Furthermore stability of the composite retains in solutions with pH from 2 to 8.

2.4 Bacteria detection

Nowadays, pathogens affect the water quality of rivers and streams in many parts of the world. Lifted up levels of E. Coli in United States (*Watershed Assessment, Tracking & Environmental Results*. Washington DC: USEPA) demonstrated that understanding the variation mechanism of these kind of pathogens is essential for diminishing the contamination of water. With new improvements in technology, studies have pointed out the great diversity of E. Coli strains in the environment [82]

These variations have been defined by the impact of genotypic and phenotypic characters of pathogens. Surviving and growth mechanism of bacteria is related with the surface feature such as lipopolysaccharides (LPS), hydrophobicity and net charge.

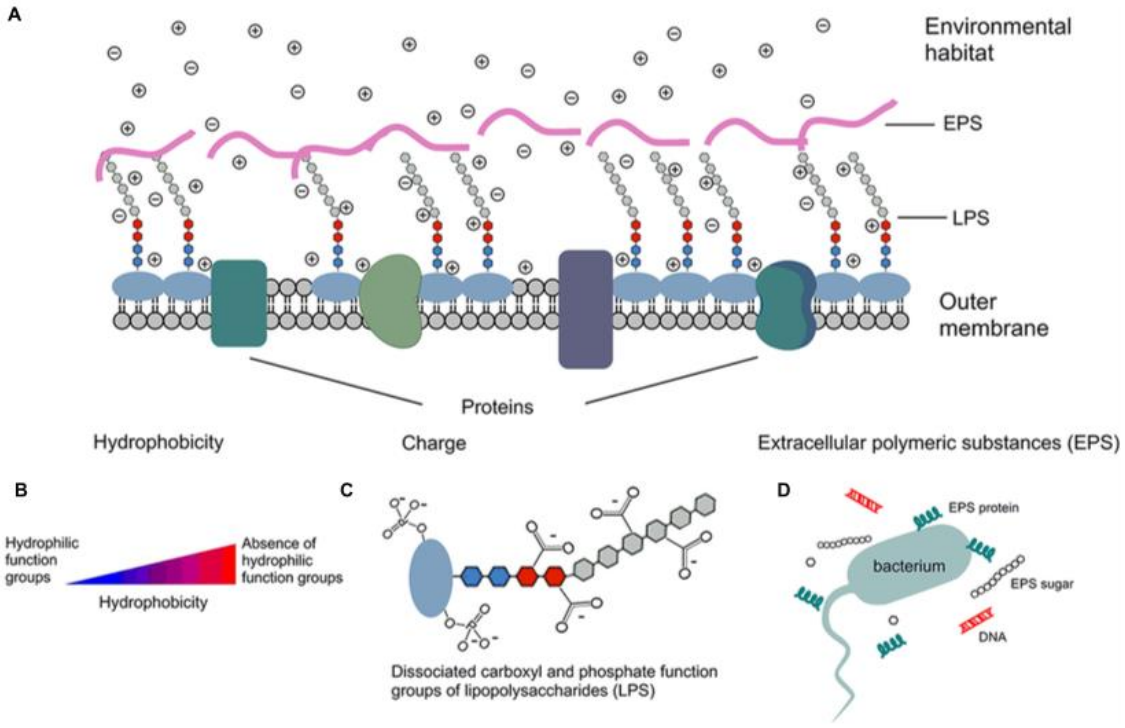

Figure 2.4.1Schematic illustration of surface characteristics of E. Coli [83]

E. coli surface on account of peptidoglycan and LPS on cell wall is negatively charged [84]. The habitat of pathogens determines the magnitude of surface charge and hydrophobicity [85] which affects the attraction and repulsion of particles. Ca^{2+} and Mg^{2+} cations could raise the hydrophobicity by binding to membrane proteins of pathogen [86].

Extracellular polymeric substances (EPS) produced by bacteria construct the outer cell surface and mainly consist of polysaccharides, proteins and DNA, lipid in small amount. EPS by providing heterogeneity actively contribute to biofilm production, cell adhesion, protection from microenvironment [83].

Mechanism of bacterial attachment is based on motile and unmotile types of microorganism. Motile pathogens occupy different depth of microenvironment: liquid with no effect from surface, near surface with hydrodynamic effect, surface with effect of electrostatic forces [87]

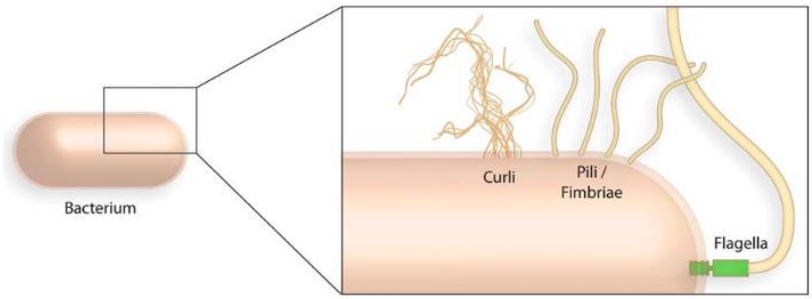

Figure 2.4.2 Bacteria organelles which enable the surface interaction [88]

Location of pathogen in fluid region is related to flagella which is the motion organelle of bacteria. E. Coli with flagella have the capacity to move through different depths in liquid. Upon contacting target surface of liquid, attachment of cellular components occurs in two ways. Reversible attachment is a kind of hydrodynamic and electrostatic interaction like polystyrene bead contact to the surface [89].

Bacteria mostly with negative surface charge particularly in stationary phase are affected by positively charged surfaces. Upon sensing quorum, E. Coli raises up the negative charge on the membrane during biofilm generation [90].

2.5 Experimental

2.5.1 Materials and Characterization Techniques

Ammonium hydroxide, TEOS, APTES and sulfur powder, polystrene were purchased from Sigma Aldrich. E. Coli DH5 Alpha strain expressing green fluorescent protein (GFP) was prepared by Synhetic biosystem research group (Urartu Şeker). Characterization techniques and instruments used in this part were described in chapter 1. In adddition, fluorescence spectrophotometer (Bilkent-UNAM) was utilized to illustrate the biosensing images.

2.5.2 Silica dots

15 ml ammonium hydroxide and 125 ml ethanol were mixed in a 100 ml glass bottle. After stirred on hot plate for 5 min (40 °C), 5 ml TEOS was added and silica dots formed with overnight stirring process. With 1 hour time interval, 2.5 ml TEOS and 0.2 ml APTES were added into mixture. Incubation for 6 hour helped to form ligand attached silica dots. 3 times washed silica dots (ethanol/water 1:3 v/v centrifuged at 5000 rpm for 5 min) were weighted at last washing process. Approximately 1.5 g silica dot was obtained. Then, they were dissolved in water and to separate the aggregated dots sonicator was used.

2.5.3 Silica coated QDs

50 mg WQD and 1g silica dot were dissolved in 100 ml deionized water and stirred on hot plate for 2 minutes. Negative and positive charge attraction caused an adherance of aqueous QDs onto silica surface. New product SQ was precipitated with ethanol/water 1:2 (v/v) at 5000 rpm for 5 min. For extra silica layer covering, precipitated SQ was dissolved in 20 ml di-water and 66 ul APTES, 1600 ul TEOS, 30 ml ethanol were added into mixture. Following stirring for 4 hour at 25 °C, product called as SCQD was washed with ethanol/water (1:2 (v/v) at 5000 rpm for 5 min). Dried SCQD particles were stored at +4 °C for further applications.

2.5.4 Polymeric film & Bacteria detection

Polymeric film was prepared by dissolving 10 g polystyrene (PS) in 100 ml chloroform (10%). PS solution was stirred overnight at room temperature. For QD film formation,

200 mg Silica-QDs was mixed with 4 ml PS polymer and then 400 ul taken from this mixture was poured onto glass. Spin coating process was applied to obtain thin films (at 1000 rpm for 30 sec). Stock of DH5 Alpha strain producing GFP protein was dissolved and grown in petri dishes with Luria broth nutrient rich media at 30 °C (overnight).

2.6 RESULTS AND DISCUSSIONS

After phase transfer, aqueous QDs were prepared for biosensing. In this part of study, silica capped QD generation process was applied and SEM images showed the scan of the PS film with magnifying (10.000x) of SCQD structure. Each round shape illustrates the silica dots with 500 nm sized approximately.

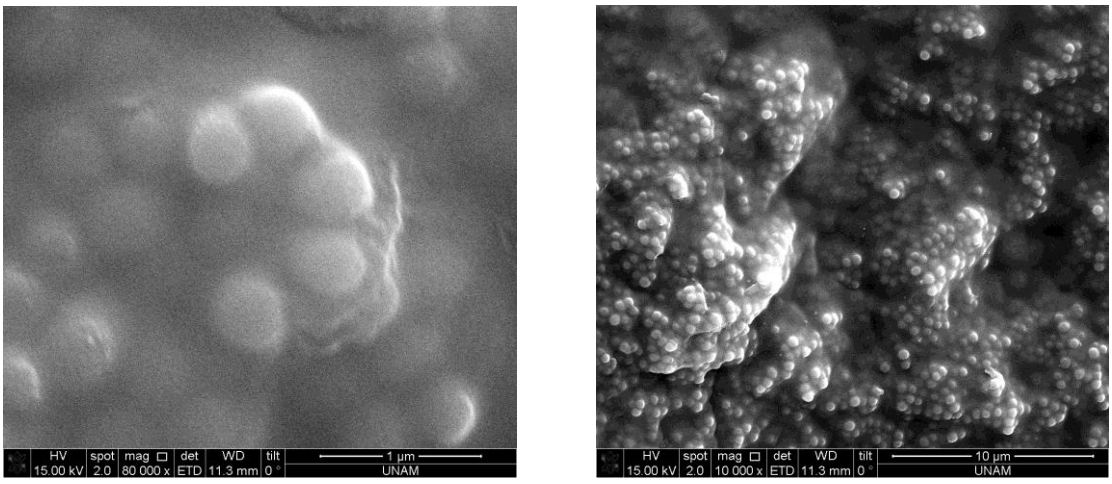

Figure 2.6.1 SEM image demonstrating the silica QDs on PS film

To understand the proper covering of QDs with SiO_2, SEM elemental analysis was done. Atomic percentages on the table show that Si, C and O are the fundamental elements for silica generation. Furthermore, CI element is core material of QDs. SEM analysis only indicated silica dots but aqueous QDs could not be seen due to their small size compared to silica dots (Figure 2.6.1).

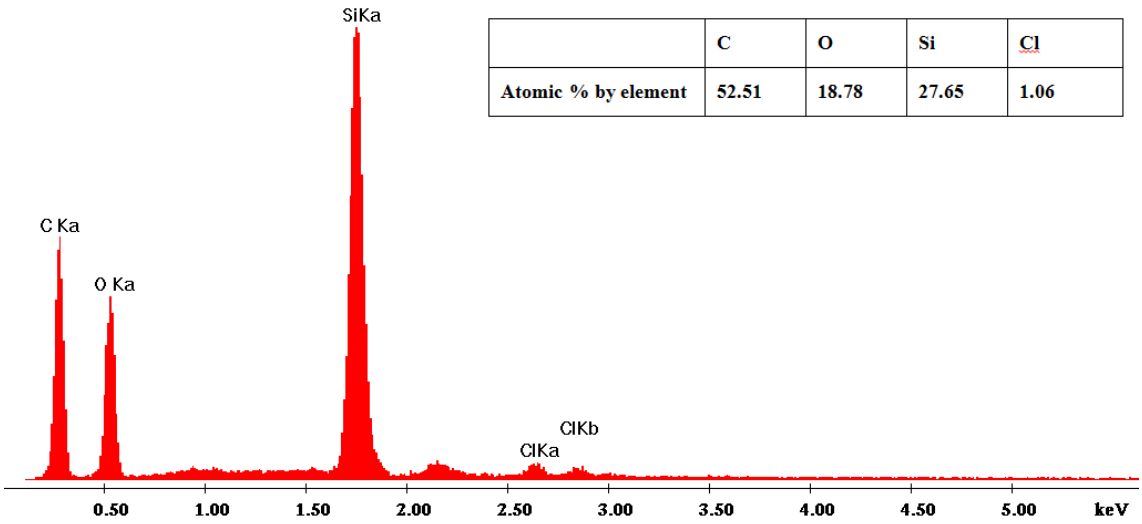

	C	O	Si	Cl
Atomic % by element	52.51	18.78	27.65	1.06

Figure 2.6.2 Elemental distribution of SCQD in SEM

To confirm the proper attachment of QDs onto silica dots, TEM was performed. Firstly, aqueous InP/ZnS QDs were detected in 5 nm and 20 nm scale bars. 3.4 nm sized aqueous QDs were clearly detected with 5nm scale bar (2.6.3).

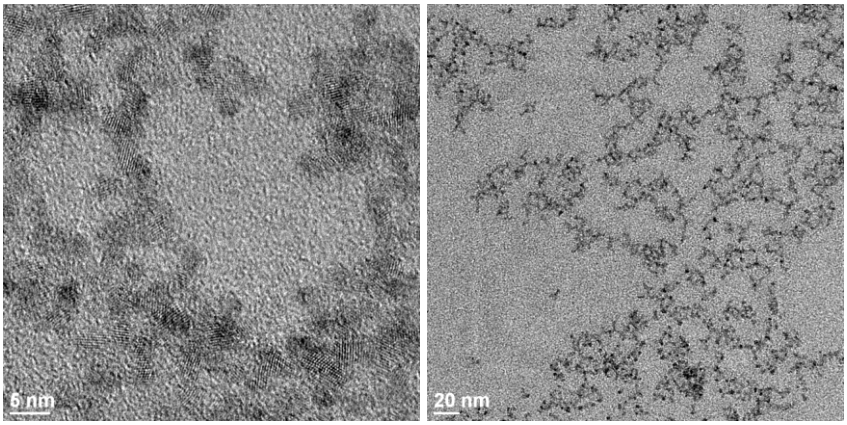

Figure 2.6.3 TEM images of aqueous QDs with 5 nm and 20 nm scale bars

Attached QDs onto SiO_2 was seen clearly with TEM instrument. Silica dot size is around 350 nm. In 10 nm scale bar image, small dots on the silica dot surface indicate very well conjugation of QDs onto silica material (Figure 2.6.4).

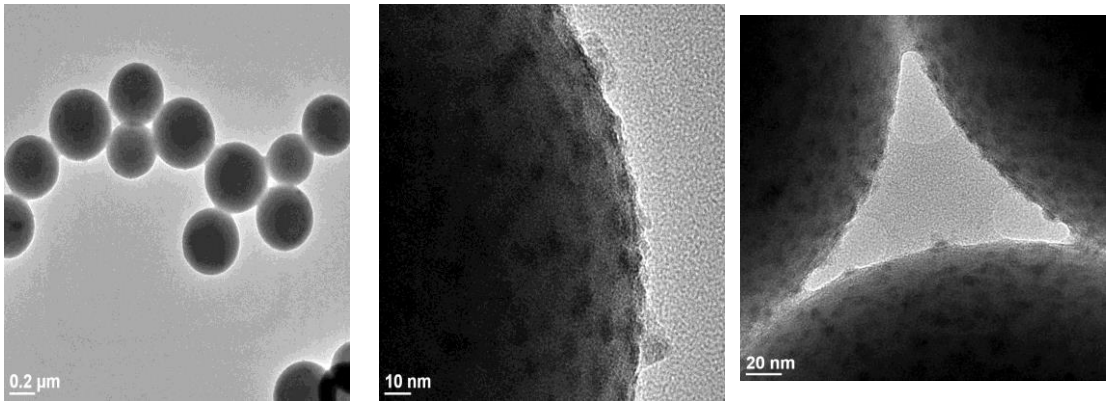

Figure 2.6.4 TEM images of silica capped QDs

After silica capped QD (SCQD) structure was well defined, bacteria detection with SCQD on film was performed. To understand the conjugation of bacteria onto SCQD in film, time resolved analysis was performed. Fluorescence time of SCQD film with emission at 620 nm was quite changed by attachment of E. Coli onto SCQD spheres (Figure 2.6.5).

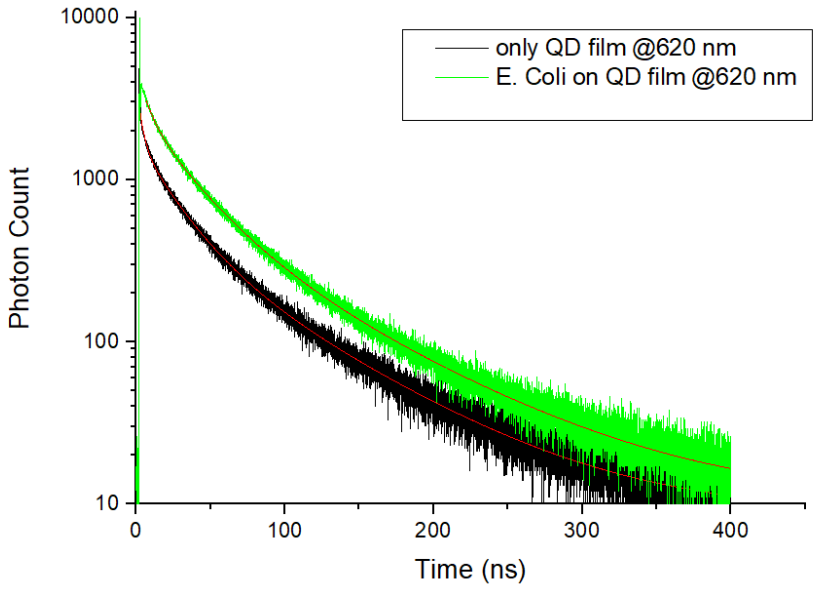

Figure 2.6.5 Time resolved spectra of SCQD film and E. Coli attached onto SCQD film

Table 2.6.1 The lifetime components of SCQD film and E. Coli attached SCQD film

Sample	A1	T1 (ns)	A2	T2 (ns)	A3	T3 (ns)	Tavg (ns)
SCQD film	1161.1 ±31.8	29.607 ±0.517 **44.38%**	994 ±119	6.945 ±0.879 **38.00%**	460.9 ±10.3	75.47 ±1.20 **17.62%**	29.077
SCQD film +E. coli	1647.6 ±31.8	29.607 ±0.517 **53.53%**	811.8 ±84.2	6.945 ±0.879 **26.37%**	618.7 ±11.5	84.32 ±1.06 **20.10%**	34.628

SCQD film and attached E. Coli were compared according to their emission time capacity (TRPL) which is related to measure the fast charge carrier dynamics. As demonstrated in Table 2.6.1, life time of both samples have three components in which the percentages of each of them differs. SCQD film T1,T2 and T3 values were recorded as 44.38, 38, 17.62 % respectively. On the contrary, percentages in SCQD attached E. Coli was seen as 53.53, 26.37, 20.10 %. Average T values were also different, changes in life time components showed the difference between SCQD and bacteria attached SCQD film. Time dependent photon delay time goes up to 34.628 ns. This mechanism could be explained by a physical energy transfer also called as fluorescence resonance energy tranfer (FRET). This distance dependent physical interaction allows passage of energy from donor to acceptor molecule. GFP expressed DH5 alpha strain have emission capacity around 530 nm and SCQD emits red color at 620 nm. Assuming that GFP with high energy could donate its energy into QD with relatively lower energy as acceptor. Therefore, this interaction might alters the delay time of QDs embedded into silica film.

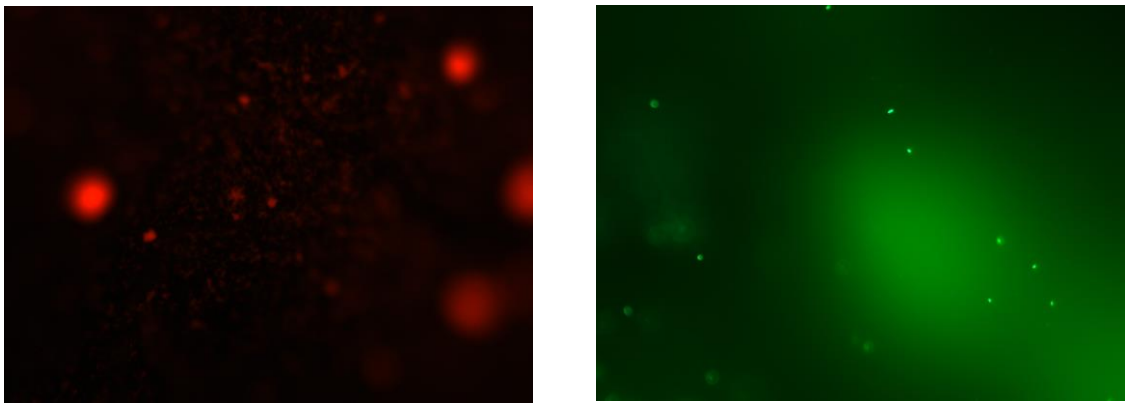

Figure 2.6.6 Fluorescence microscope image of a. SCQD film prepared by polyvinylalcohol (PVA) and water b. GFP expressed E. Coli on SCQD film (PVA and water)

Polymer of SCQD firstly made by PVA and water which is environmental and easily disposable. However its endurance to bacteria environment is rather low and dissolves in a short time. Therefore, a water resist polymer was needed for biosensing approach. For the further detection, polystyrene was prepared in chloroform and QDs were embedded into this film (Figure 2.6.6).

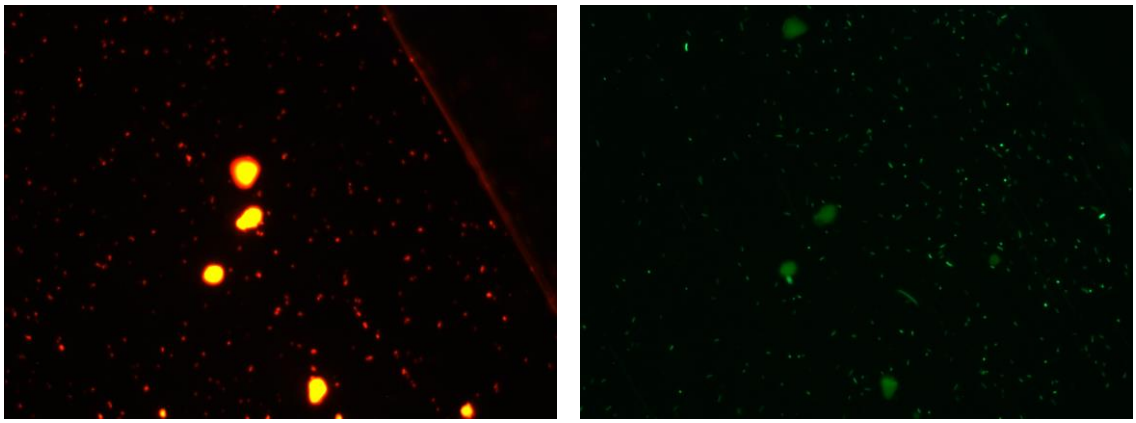

Figure 2.6.7 Fluorescence microscope image of a. SCQD film (prepared by PS and chloroform) with emission at 620 nm b. GFP expressed E. Coli on SCQD film with 530 nm emission wavelength

As seen in Figure 2.6.7, attraction of E. Coli from SCQD was clearly observed by fluorescence microscope. E. Coli with negative charge attracted positively charged SCQD. Van der waals forces are essential for the assembling of this pathogen onto SCQD film (The image was taken from the same position by only changing excitation wavelength to detect both QDs and DH5 alpha).

2.7 CONCLUSION and FUTURE PERSPECTIVE

The main target of this thesis is the rapid and simple paper based detection of bacteria by using silica covered QDs. Nowadays pathogen toxicity in water threatens lives in cities and villages. Therefore, quick detection of toxic and harmful substance have critical role in rescue and raise the quality of life.

Biosensing approach by using high fluorescence emitting QDs was investigated. Currently, many studies in biofield are based on formation and application of environmental and less toxic materials onto biosystems. Therefore, cadmium free materials are essential factor in bioapplications. These semiconductor nanocrystals have size tuning capability so halide precursor changing results in differences in emission wavelength. In addition, high and relatively more stable PLQY compared to biological dyes gave an opportunity to QDs entering into biotreatments.

In this study best QY (50%) and FWHM 56 (nm) were obtained in red emitting InP/ZnS QDs due to excitation with variable energy states and also red QD stability directs many studies currently. As mentioned in result part, QDs synthesized with interested PLQY and FWHM and chemical yield were then functionalized for the utilization of QDs on bacteria detection. Following phase transfer, PLQY was decreased to 20% owing to insufficient surface passivation by removing TOP-S ligands. However, stability was maintained by covering aqueous QDs with SiO_2. With the TEM analysis approval, SCQD generation was proved. As a sample pathogen, DH5 Alpha expressing GFP was used. SCQD QDs with NH_2 groups on the surface attracted negatively charged gram negative E. Coli pathogen with having LPS on its membrane. It is expected that this study can pave the way for rapid and efficient detection of pathogens.

BIBLIOGRAPHY

[1] N. Yaacobi-Gross, M. Soreni-Harari, M. Zimin, S. Kababya, A. Schmidt, and N. Tessler, "Molecular control of quantum-dot internal electric field and its application to CdSe-based solar cells," *Nature Materials*, vol. 10, no. 12, pp. 974–979, 2011.

[2] B. Dubertret, "In Vivo Imaging of Quantum Dots Encapsulated in Phospholipid Micelles," *Science*, vol. 298, no. 5599, pp. 1759–1762, 2002.

[3] K. Roy Choudhury, Y. Sahoo, T. Y. Ohulchanskyy, and P. N. Prasad, "Efficient photoconductive devices at infrared wavelengths using quantum dot-polymer nanocomposites," *Applied Physics Letters*, vol. 87, no. 7, 2005.

[4] E. A.A.Onushchenko, "Quantum size effect in three-dimensional micorscopic semiconductor crystals," *Jetp Letters*, vol. 34. pp. 345–349, 1981.

[5] C. B. Murray, C. R. Kagan, and M. G. Bawendi, "Synthesis and Characterization of Monodisperse Nanocrystals and Close-Packed Nanocrystal Assemblies," *Annual Review of Materials Science*, vol. 30, no. 1, pp. 545–610, 2000.

[6] C. B. Murray, D. J. Norris, and M. G. Bawendi, "Synthesis and characterization of nearly monodisperse CdE (E = sulfur, selenium, tellurium) semiconductor nanocrystallites," *Journal of the American Chemical Society*, vol. 115, no. 19, pp. 8706–8715, 1993.

[7] J. J. Li *et al.*, "Large-scale synthesis of nearly monodisperse CdSe/CdS core/shell nanocrystals using air-stable reagents via successive ion layer adsorption and reaction," *Journal of the American Chemical Society*, vol. 125, no. 41, pp. 12567–12575, 2003.

[8] Y. Zheng, S. Gao, and J. Y. Ying, "Synthesis and cell-imaging applications of glutathione-capped CdTe quantum dots," *Advanced Materials*, vol. 19, no. 3, pp. 376–380, 2007.

[9] G. Konstantatos and E. H. Sargent, *Colloidal Quantum Dot Optoelectronics and Photovoltaics*, 2013th ed. CUP.

[10] J. Park, J. Joo, G. K. Soon, Y. Jang, and T. Hyeon, "Synthesis of monodisperse spherical nanocrystals," *Angewandte Chemie - International Edition*, vol. 46, no. 25. pp. 4630–4660, 2007.

[11] I. M. Lifshitz and V. V. Slyozov, "The kinetics of precipitation from supersaturated solid solutions," *Journal of Physics and Chemistry of Solids*, vol. 19, no. 1–2, pp. 35–50, 1961.

[12] I. U. Arachchige and M. G. Kanatzidis, "Anomalous band gap evolution from band inversion in Pb 1-xSn xTe nanocrystals," *Nano Letters*, vol. 9, no. 4, pp. 1583–1587, 2009.

[13] A. Glaria *et al.*, "An organometallic approach for very small maghemite nanoparticles: Synthesis, characterization, and magnetic properties," *ChemPhysChem*, vol. 9, no. 14, pp. 2035–2041, 2008.

[14] Z. a Peng and X. Peng, "Nearly monodisperse and shape controlled CdSe nanocrystals via alternative routes: nucleation and growth," *J. Am. Chem. Soc.*, vol. 124, no. 8, p. 3343, 2002.

[15] L. Li and P. Reiss, "One-pot synthesis of highly luminescent InP/ZnS nanocrystals without precursor injection," *Journal of the American Chemical Society*, vol. 130, no. 35, pp. 11588–11589, 2008.

[16] O. I. Micic, C. J. Curtis, K. M. Jones, J. R. Sprague, and A. J. Nozik, “Synthesis and Characterization of InP Quantum Dots,” *The Journal of Physical Chemistry*, vol. 98, no. 19, pp. 4966–4969, 1994.
[17] M. Yarema, M. V. Kovalenko, G. Hesser, D. V. Talapin, and W. Heiss, “Highly monodisperse bismuth nanoparticles and their three-dimensional superlattices,” *Journal of the American Chemical Society*, vol. 132, no. 43, pp. 15158–15159, 2010.
[18] J. B. Hoffman, R. Alam, and P. V. Kamat, “Why Surface Chemistry Matters for QD–QD Resonance Energy Transfer,” *ACS Energy Letters*, pp. 391–396, 2017.
[19] A. Zabet-Khosousi and A.-A. Dhirani, “Charge Transport in Nanoparticle Assemblies,” *Chemical Reviews*, vol. 108, no. 10, pp. 4072–4124, 2008.
[20] M. Kuno, J. K. Lee, B. O. Dabbousi, F. V. Mikulec, and M. G. Bawendi, “The band edge luminescence of surface modified CdSe nanocrystallites: Probing the luminescing state,” *The Journal of Chemical Physics*, vol. 106, no. 23, pp. 9869–9882, 1997.
[21] J. A. Dahl, B. L. S. Maddux, and J. E. Hutchison, “Toward greener nanosynthesis,” *Chemical Reviews*, vol. 107, no. 6. pp. 2228–2269, 2007.
[22] N. Gaponik *et al.*, “Thiol-capping of CDTe nanocrystals: An alternative to organometallic synthetic routes,” *Journal of Physical Chemistry B*, vol. 106, no. 29, pp. 7177–7185, 2002.
[23] J. S. Owen, J. Park, P. E. Trudeau, and A. P. Alivisatos, “Reaction chemistry and ligand exchange at cadmium-selenide nanocrystal surfaces,” *Journal of the American Chemical Society*, vol. 130, no. 37, pp. 12279–12281, 2008.
[24] G. Konstantatos and E. H. Sargent, *Colloidal Quantum Dot Optoelectronics and Photovoltaics*, 2013th ed. CUP.
[25] D. C. Oertel, M. G. Bawendi, A. C. Arango, and V. Bulović, “Photodetectors based on treated CdSe quantum-dot films,” *Applied Physics Letters*, vol. 87, no. 21, pp. 1–3, 2005.
[26] M. Law, J. M. Luther, Q. Song, B. K. Hughes, C. L. Perkins, and A. J. Nozik, “Structural, optical, and electrical properties of PbSe nanocrystal solids treated thermally or with simple amines,” *Journal of the American Chemical Society*, vol. 130, no. 18, pp. 5974–5985, 2008.
[27] E. H. Sargent, “Solar cells, photodetectors, and optical sources from infrared colloidal quantum dots,” *Advanced Materials*, vol. 20, no. 20, pp. 3958–3964, 2008.
[28] J. Liu, T. Tanaka, K. Sivula, A. P. Alivisatos, and J. M. J. Fréchet, “Employing end-functional polythiophene to control the morphology of nanocrystal - Polymer composites in hybrid solar cells,” *Journal of the American Chemical Society*, vol. 126, no. 21, pp. 6550–6551, 2004.
[29] A. Nag, M. V. Kovalenko, J. S. Lee, W. Liu, B. Spokoyny, and D. V. Talapin, “Metal-free inorganic ligands for colloidal nanocrystals: S2-, HS-, Se2-, HSe-, Te2-, HTe -, TeS32-, OH-, and NH 2- as surface ligands,” *Journal of the American Chemical Society*, vol. 133, no. 27, pp. 10612–10620, 2011.
[30] M. V. Kovalenko *et al.*, “Prospects of nanoscience with nanocrystals,” *ACS Nano*, vol. 9, no. 2, pp. 1012–1057, 2015.
[31] A. Dong *et al.*, “A generalized ligand-exchange strategy enabling sequential surface functionalization of colloidal nanocrystals,” *Journal of the American Chemical Society*, vol. 133, no. 4, pp. 998–1006, 2011.
[32] Y. Altintas, M. Y. Talpur, M. Unlu, and E. Mutlugun, “Highly Efficient Cd-Free Alloyed Core/Shell Quantum Dots with Optimized Precursor Concentrations,”

Journal of Physical Chemistry C, vol. 120, no. 14, pp. 7885–7892, 2016.
[33] D. E. Gómez, M. Califano, and P. Mulvaney, "Optical properties of single semiconductor nanocrystals.," *Physical chemistry chemical physics : PCCP*, vol. 8, no. 43, pp. 4989–5011, 2006.
[34] O. V. Prezhdo, "Photoinduced dynamics in semiconductor quantum Dots: Insights from time-domain ab initio studies," *Accounts of Chemical Research*, vol. 42, no. 12, pp. 2005–2016, 2009.
[35] O. Madelung, "Semiconductors: Data Handbook; Ix - VIy compounds," in *Semiconductors: Data Handbook 3rd Ed.*, 2004, pp. 220–235.
[36] E. Mutlugun *et al.*, "Large-Area (over 50 cm × 50 cm) freestanding films of colloidal InP/ZnS quantum dots," *Nano Letters*, vol. 12, no. 8, pp. 3986–3993, 2012.
[37] C. de Mello Donegá and R. Koole, "Size Dependence of the Spontaneous Emission Rate and Absorption Cross Section of CdSe and CdTe Quantum Dots," *The Journal of Physical Chemistry C*, vol. 113, no. 16, pp. 6511–6520, 2009.
[38] L. Qu, Z. A. Peng, and X. Peng, "Alternative Routes toward High Quality CdSe Nanocrystals," *Nano Letters*, vol. 1, no. 6, pp. 333–337, 2001.
[39] M. Nirmal, C. B. Murray, and M. G. Bawendi, "Fluorescence-line narrowing in CdSe quantum dots: Surface localization of the photogenerated exciton," *Physical Review B*, vol. 50, no. 4, pp. 2293–2300, 1994.
[40] D. J. Norris and M. G. Bawendi, "Measurement and assignment of the size-dependent optical spectrum in CdSe quantum dots," *Physical Review B*, vol. 53, no. 24, pp. 16338–16346, 1996.
[41] M. A. Hines and P. Guyot-Sionnest, "Synthesis and Characterization of Strongly Luminescing ZnS-Capped CdSe Nanocrystals," *The Journal of Physical Chemistry*, vol. 100, no. 2, pp. 468–471, 1996.
[42] J. Yao, D. R. Larson, H. D. Vishwasrao, W. R. Zipfel, and W. W. Webb, "Blinking and nonradiant dark fraction of water-soluble quantum dots in aqueous solution," *Proceedings of the National Academy of Sciences*, vol. 102, no. 40, pp. 14284–14289, 2005.
[43] V. Brunetti *et al.*, "InP/ZnS as a safer alternative to CdSe/ZnS core/shell quantum dots: in vitro and in vivo toxicity assessment," *Nanoscale*, vol. 5, no. 1, pp. 307–317, 2013.
[44] R. Xie, D. Battaglia, and X. Peng, "Colloidal InP nanocrystals as efficient emitters covering blue to near-infrared," *Journal of the American Chemical Society*, vol. 129, no. 50, pp. 15432–15433, 2007.
[45] P. Yan, Y. Xie, W. Wang, F. Liu, and Y. Qian, "A low-temperature route to InP nanocrystals," *Journal of Materials Chemistry*, vol. 9, pp. 1831–1833, 1999.
[46] Z. Liu, A. Kumbhar, D. Xu, J. Zhang, Z. Sun, and J. Fang, "Coreduction colloidal synthesis of III-V nanocrystals: the case of InP," *Angewandte Chemie - International Edition*, vol. 47, no. 19, pp. 3540–3542, 2008.
[47] J. Lauth, T. Strupeit, A. Kornowski, and H. Weller, "A transmetalation route for colloidal GaAs nanocrystals and additional III-V semiconductor materials," *Chemistry of Materials*, vol. 25, no. 8, pp. 1377–1383, 2013.
[48] M. D. Tessier, D. Dupont, K. De Nolf, J. De Roo, and Z. Hens, "Economic and Size-Tunable Synthesis of InP / ZnE (E=S, Se) Colloidal Quantum Dots.," *Chemistry of Materials*, vol. 27, pp. 4893–4898, 2015.
[49] D. Su *et al.*, "Dark to light! A new strategy for large Stokes shift dyes: coupling of a dark donor with tunable high quantum yield acceptors," *Chem. Sci.*, vol. 5, no. 12, pp. 4812–4818, 2014.

[50] M. Meyer, C. Wallberg, K. Kurihara, and J. H. Fendler, “Photosensitized charge separation and hydrogen production in reversed micelle entrapped platinized colloidal cadmium sulphide,” *Journal of the Chemical Society, Chemical Communications*, no. 2, pp. 90–91, 1984.
[51] A. Henglein, “Mechanism of reactions on colloidal microelectrodes and size quantization effects,” *Electrochemistry II, Topics In Current Chemistry, Vol. 143*, vol. 143, pp. 113–180, 1988.
[52] D. Schooss, A. Mews, A. Eychmüller, and H. Weller, “Quantum-dot quantum well CdS/HgS/CdS: Theory and experiment,” *Physical Review B*, vol. 49, no. 24, pp. 17072–17078, 1994.
[53] A. L. Rogach, L. Katsikas, A. Kornowski, D. Su, A. Eychmuller, and H. Weller, “Synthesis, morphology and optical properties of thiol-stabilized CdTe nanoclusters in aqueous solution,” *Berichte der Bunsengesellschaft/Physical Chemistry Chemical Physics*, vol. 101, no. 11, pp. 1668–1670, 1997.
[54] Y. Li, L. Jing, R. Qiao, and M. Gao, “Aqueous synthesis of CdTe nanocrystals: progresses and perspectives,” *Chemical Communications*, vol. 47, no. 33, p. 9293, 2011.
[55] A. L. Rogach *et al.*, “Aqueous synthesis of thiol-capped CdTe nanocrystals: State-of-the-art,” *Journal of Physical Chemistry C*, vol. 111, no. 40, pp. 14628–14637, 2007.
[56] S. V. Kershaw, A. S. Susha, and A. L. Rogach, “Narrow bandgap colloidal metal chalcogenide quantum dots: synthetic methods, heterostructures, assemblies, electronic and infrared optical properties,” *Chemical Society Reviews*, vol. 42, no. 7, p. 3033, 2013.
[57] I. L. Medintz, H. T. Uyeda, E. R. Goldman, and H. Mattoussi, “Quantum dot bioconjugates for imaging, labelling and sensing,” *Nature Materials*, vol. 4, no. 6, pp. 435–446, 2005.
[58] X. Michalet *et al.*, “Quantum Dots for Live Cells, in Vivo Imaging, and Diagnostics,” *Science (Washington, DC, United States)*, vol. 307, no. 5709, pp. 538–544, 2005.
[59] E. H. Sargent, “Infrared quantum dots,” *Advanced Materials*, vol. 17, no. 5, pp. 515–522, 2005.
[60] X. Peng *et al.*, “Shape control of CdSe nanocrystals,” *Nature*, vol. 404, no. 6773, pp. 59–61, 2000.
[61] W. W. Yu, Y. a Wang, and X. G. Peng, “Formation and stability of size-, shape-, and structure-controlled CdTe nanocrystals: ligand effects …,” *Chem. Mater*, no. 24, pp. 4300–4308, 2003.
[62] J. Zhou, Y. Yang, and C. Y. Zhang, “Toward Biocompatible Semiconductor Quantum Dots: From Biosynthesis and Bioconjugation to Biomedical Application,” *Chemical Reviews*, vol. 115, no. 21, pp. 11669–11717, 2015.
[63] R. Cui *et al.*, “Living yeast cells as a controllable biosynthesizer for fluorescent quantum dots,” *Advanced Functional Materials*, vol. 19, no. 15, pp. 2359–2364, 2009.
[64] N. Ma, T. Grigory, and S. O. Kelley, “Nucleic acid-passivated semiconductor nanocrystals: Biomolecular templating of form and function,” *Accounts of Chemical Research*, vol. 43, no. 2, pp. 173–180, 2010.
[65] N. Ma, E. H. Sargent, and S. O. Kelley, “One-step DNA-programmed growth of luminescent and biofunctionalized nanocrystals,” *Nature Nanotechnology*, vol. 4, no. 2, pp. 121–125, 2009.
[66] A. L. Rogach, L. Katsikas, A. Kornowski, S. Dangsheng, A. Eychmüller, and H.

Weller, “Synthesis and characterization of thiol-stabilized CdTe nanocrystals,” *Ber. Bunsen Phys. Chem.*, vol. 100, no. 11, pp. 1772–1778, 1996.
[67] M. Gao *et al.*, “Strongly Photoluminescent CdTe Nanocrystals by Proper Surface Modification,” *The Journal of Physical Chemistry B*, vol. 102, no. 43, pp. 8360–8363, 1998.
[68] H. Zhang, Z. Zhou, B. Yang, and M. Gao, “The influence of carboxyl groups on the photoluminescence of mercaptocarboxylic acid-stabilized CdTe nanoparticles,” *Journal of Physical Chemistry B*, vol. 107, no. 1, pp. 8–13, 2003.
[69] I. L. Medintz, A. R. Clapp, H. Mattoussi, E. R. Goldman, B. Fisher, and J. M. Mauro, “Self-assembled nanoscale biosensors based on quantum dot FRET donors,” *Nature Materials*, vol. 2, no. 9, pp. 630–638, 2003.
[70] H. Mattoussi, M. Kenneth Kuno, E. R. Goldman, G. P. Anderson, and J. Matthew Mauro, *Optical Biosensors*. 2002.
[71] F. Pinaud, D. King, H. P. Moore, and S. Weiss, “Bioactivation and Cell Targeting of Semiconductor CdSe/ZnS Nanocrystals with Phytochelatin-Related Peptides,” *Journal of the American Chemical Society*, vol. 126, no. 19, pp. 6115–6123, 2004.
[72] E. R. Goldman, G. P. Anderson, P. T. Tran, H. Mattoussi, P. T. Charles, and J. M. Mauro, “Conjugation of luminescent quantum dots with antibodies using an engineered adaptor protein to provide new reagents for fluoroimmunoassays,” *Analytical Chemistry*, vol. 74, no. 4, pp. 841–847, 2002.
[73] K. I. Hanaki *et al.*, “Semiconductor quantum dot/albumin complex is a long-life and highly photostable endosome marker,” *Biochemical and Biophysical Research Communications*, vol. 302, no. 3, pp. 496–501, 2003.
[74] P. T. Snee, R. C. Somers, G. Nair, J. P. Zimmer, M. G. Bawendi, and D. G. Nocera, “A ratiometric CdSe/ZnS nanocrystal pH sensor,” *Journal of the American Chemical Society*, vol. 128, no. 41, pp. 13320–13321, 2006.
[75] Y. Yang, Z. Wen, Y. Dong, and M. Gao, “Incorporating CdTe nanocrystals into polystyrene microspheres: Towards robust fluorescent beads,” *Small*, vol. 2, no. 7, pp. 898–901, 2006.
[76] T. Nann and P. Mulvaney, “Single quantum dots in spherical silica particles,” *Angewandte Chemie - International Edition*, vol. 43, no. 40, pp. 5393–5396, 2004.
[77] B. Ji *et al.*, “Non-blinking quantum dot with a plasmonic nanoshell resonator,” *Nature Nanotechnology*, vol. 10, no. 2, pp. 170–175, 2015.
[78] Z. Lin, X. Fei, Q. Ma, X. Gao, and X. Su, “$CuInS_2$ quantum dots@silica near-infrared fluorescent nanoprobe for cell imaging,” *New J. Chem.*, vol. 38, no. 1, pp. 90–96, 2014.
[79] M. Szekeres, J. Tóth, and I. Dékány, “Specific surface area of stoeber silica determined by various experimental methods,” *Langmuir*, vol. 18, no. 7, pp. 2678–2685, 2002.
[80] L. Jing *et al.*, “Highly fluorescent CdTe@SiO2 particles prepared via reverse microemulsion method,” *Chemistry of Materials*, vol. 22, no. 2, pp. 420–427, 2010.
[81] Z. Ran and W. Yang, “Silica/CdTe/Silica Fluorescent Composite Nanoparticles via Electrostatic Assembly as a pH Ratiometer,” *RSC Advances*, vol. 4, no. 71, pp. 37921–37927, 2014.
[82] K. L. Cook, C. H. Bolster, K. A. Ayers, and D. N. Reynolds, “Escherichia coli diversity in livestock manures and agriculturally impacted stream waters,” *Current Microbiology*, vol. 63, no. 5, pp. 439–449, 2011.

[83] C. G. Bruckner, C. Rehm, H. P. Grossart, and P. G. Kroth, “Growth and release of extracellular organic compounds by benthic diatoms depend on interactions with bacteria,” *Environmental Microbiology*, vol. 13, no. 4, pp. 1052–1063, 2011.

[84] R. M. Goulter, I. R. Gentle, and G. A. Dykes, “Issues in determining factors influencing bacterial attachment: A review using the attachment of Escherichia coli to abiotic surfaces as an example,” *Letters in Applied Microbiology*, vol. 49, no. 1. pp. 1–7, 2009.

[85] J. B. Fein, J. F. Boily, N. Yee, D. Gorman-Lewis, and B. F. Turner, “Potentiometric titrations of Bacillus subtilis cells to low pH and a comparison of modeling approaches,” *Geochimica et Cosmochimica Acta*, vol. 69, no. 5, pp. 1123–1132, 2005.

[86] W. Khemakhem, E. Ammar, and A. Bakhrouf, “Effect of environmental conditions on hydrophobicity of marine bacteria adapted to textile effluent treatment,” *World Journal of Microbiology and Biotechnology*, vol. 21, no. 8–9, pp. 1623–1631, 2005.

[87] M. A. S. Vigeant, R. M. Ford, M. Wagner, and L. K. Tamm, “Reversible and irreversible adhesion of motile Escherichia coli cells analyzed by total internal reflection aqueous fluorescence microscopy,” *Applied and Environmental Microbiology*, vol. 68, no. 6, pp. 2794–2801, 2002.

[88] H. H. Tuson and D. B. Weibel, “Bacteria–surface interactions,” *Soft Matter*, vol. 9, no. 17, p. 4368, 2013.

[89] J. M. Meinders, H. C. van der Mei, and H. J. Busscher, “Deposition Efficiency and Reversibility of Bacterial Adhesion under Flow,” *Journal of Colloid and Interface Science*, vol. 176, no. 2, pp. 329–341, 1995.

[90] K. E. Eboigbodin, J. R. A. Newton, A. F. Routh, and C. A. Biggs, “Bacterial quorum sensing and cell surface electrokinetic properties,” *Applied Microbiology and Biotechnology*, vol. 73, no. 3, pp. 669–675, 2006.